



Preparation of 3DOM ZrTiO₄ Support, W_xCeMnO₈/3DOM ZrTiO₄ Catalysts, and Their Catalytic Performance for the Simultaneous Removal of Soot and NO_x

Ruidan Wang^{1,2}, Chengming Zhong¹, Dong Li¹, Xuehua Yu^{2*}, Zhen Zhao^{1,2*}, Zbigniew Sojka³, Andrzej Kotarba³, Yuechang Wei¹ and Jian Liu¹

¹State Key Laboratory of Heavy Oil Processing, China University of Petroleum, Beijing, China, ²Institute of Catalysis for Energy and Environment, College of Chemistry and Chemical Engineering, Shenyang Normal University, Shenyang, China, ³Faculty of Chemistry, Jagiellonian University, Kraków, Poland

OPEN ACCESS

Edited by:

Laura Pastor-Pérez,
University of Seville, Spain

Reviewed by:

Jinlong Wang,
Wuhan University of Technology,
China
Yang Liu,
Dalian University of Technology, China

*Correspondence:

Xuehua Yu
yuxuehua1986@163.com
Zhen Zhao
zhenzhao@cup.edu.cn

Specialty section:

This article was submitted to
Catalytic Reactions and Chemistry,
a section of the journal
Frontiers in Chemistry

Received: 22 February 2022

Accepted: 28 March 2022

Published: 04 May 2022

Citation:

Wang R, Zhong C, Li D, Yu X, Zhao Z, Sojka Z, Kotarba A, Wei Y and Liu J (2022) Preparation of 3DOM ZrTiO₄ Support, W_xCeMnO₈/3DOM ZrTiO₄ Catalysts, and Their Catalytic Performance for the Simultaneous Removal of Soot and NO_x. *Front. Chem.* 10:880884. doi: 10.3389/fchem.2022.880884

As an efficient and durable engine, a diesel engine has a broad application. However, soot particles (PM) and nitrogen oxides (NO_x) coming from diesel engines are the main causes of air pollution, so it is necessary to design and prepare an effective catalyst for the simultaneous elimination of PM and NO_x. In this work, a novel 3DOM ZrTiO₄ support and a series of W_xCeMnO₈/3DOM ZrTiO₄ catalysts (where x indicates the wt% of W) were designed and fabricated by the colloidal crystal template technique. Among the as-prepared catalysts, the W₁CeMnO₈/3DOM ZrTiO₄ catalyst exhibits the highest NO conversion rate (52%) at the temperature of maximum CO₂ concentration (474°C) and achieves 90% NO conversion in the temperature range of 250–396°C. The excellent catalytic performance is associated with the macroporous structure, abundant oxygen vacancies, sufficient acid sites, and the synergistic effect among the active components. The possible reaction mechanisms of W_xCeMnO₈/3DOM ZrTiO₄ catalysts were also discussed based on the characterization results.

Keywords: three-dimensional ordered macroporous structure, soot particulates, nitrogen oxides, simultaneous removal, catalysts

1 INTRODUCTION

Diesel engines are ideal for heavy-duty vehicles, with high durability, lower cost, and longevity (Wei et al., 2011; Chen et al., 2016; Dai et al., 2016; Cheng et al., 2017a). However, a lot of soot particles (PM) and nitrogen oxides (NO_x) are simultaneously generated during diesel combustion (Epling et al., 2004; Liu and Gao, 2011). PM and NO_x are the main causes of urban haze weather, which can lead to serious environmental pollution and health problems (Zhu et al., 2008; Li et al., 2012; Shen et al., 2013; Choi and Lee, 2014). As more and more stringent emission standards are set by governments, there is a growing interest in developing technologies which enable the reduction of such emissions.

At present, after-treatment technologies are widely used to eliminate soot particulates and NO_x (Gogos et al., 2014; Urán et al., 2019); that is, a catalyzed diesel particulate filter (CDPF) is applied to eliminate soot particulates (Wei et al., 2011; Yu et al., 2017), and the selective catalytic reduction (SCR) technology or the nitrogen oxide storage reduction (NSR) technology is simultaneously matched for the NO_x removal

(Li et al., 2015; Li et al., 2016). However, traditionally, the after-treatment technique possesses some inherited flaws, such as big system volume, large mass, and high cost. In view of this, the idea of the concurrent catalytic elimination of soot particles and NO_x in a single trap is attractive and has been initially projected by Yoshida et al. (1989). This approach has attracted great interest from researchers, as it reduces the pressure and shrinks the volume and mass of the system. However, a few shortcomings are still there and are yet to be overcome. For example, the PM combustion process is a characteristic gas–solid–solid catalytic reaction; in general, the diameter of PM is larger than the pore diameter of conventional catalysts, so the soot particles cannot be efficiently transported through the pores of catalytic materials and the active sites cannot be fully used either. In addition, NO_x conversion takes place in a lean-burn condition, but the excessive O₂ and insufficient reductant will result in a low NO_x conversion.

Many catalysts have been developed for the simultaneous elimination of soot particulates and NO_x, such as noble metals (Serhan et al., 2019), metal oxides (Bueno-López et al., 2016; Cheng et al., 2017b), perovskite oxides (Liu et al., 2008; Li et al., 2010; Wang et al., 2010), zeolites (Fritz and Pitchon, 1997), and spinel phases (Lin et al., 2009). Among these materials, metal oxides have shown excellent performances (Li et al., 2009; Shen et al., 2013). Mn-based catalysts have been proven to be exceptional in PM combustion and SCR reactions (Chen et al., 2019; Yu D. et al., 2021; Peng et al., 2021). As a promoter, even active catalysts, namely, CeO₂-containing materials, are applied widely because of their excellent ability for oxygen storage and the aptitude to shift between Ce⁴⁺ and Ce³⁺ under a stipulated redox environment (Jin et al., 2014). Specifically, tungsten species have been reported to have the function to advance the catalytic availability of active sites, oxygen-related vacancy, and acid-introduced sites (Xiong et al., 2017). In addition, TiO₂ is always busy as support for SCR catalysts (Wu et al., 2011), and by the way, adding additional elements may increase the surface area and thermal stability, and enhance the surface acidity.

Herein, a new type of ZrTiO₄ support with a three-dimensional ordered macroporous (3DOM) structure was synthesized by the colloidal crystal templating (CCT) technique, which is rarely reported in the previous literature. Meanwhile, three cheap active elements of W, Ce, and Mn were added to the 3DOM ZrTiO₄ support by a simple and convenient method to simultaneously remove nitrogen oxides and soot particles from diesel exhausts. The as-prepared catalysts have a three-dimensional ordered, interconnected macroporous structure, which can effectively improve the contact performance between reactants and catalytic active sites, and facilitate the effective transmission of particulate reactants. NH₃ as a reducing gas was also introduced in order to improve the reduction of NO_x.

2 EXPERIMENTAL

2.1 Material Preparation

2.1.1 Synthesis of 3DOM ZrTiO₄ Support

The 3DOM ZrTiO₄ support was fabricated by the colloidal crystal templating (CCT) technique, and the template was prepared by

using polymethyl methacrylate (PMMA) spheres (Xu et al., 2011). In a typical process, C₁₆H₃₆O₄Ti and ZrOCl₂·8H₂O (at a molar ratio of 1:1) were taken in the mixed solution of methanol and ethylene glycol (at a volume ratio of 3:7), and strongly stirred followed by the addition of the PMMA template. The mixture was maintained for 3 h until the PMMA templates had been fully impregnated. The excess precursor solution was separated by vacuum filtration. Subsequently, the final precipitate was maintained at 80°C for 12 h to dry. After that, the dried precipitate was calcined at 550°C for 4 h with a raising rate of 1°C/min to remove the template. Finally, 3DOM ZrTiO₄ support was obtained.

2.1.2 Synthesis of 3DOM ZrTiO₄ Supported Catalysts

The 3DOM ZrTiO₄ supported catalysts were synthesized by the incipient wetness impregnation method. (NH₄)₆H₂W₁₂O₄₀·xH₂O, Ce(NO₃)₃·6H₂O, and Mn(NO₃)₂·4H₂O with different mass ratios were dissolved in distilled water, and then the mixture was added dropwise into the 0.5 g ZrTiO₄ support. The volume of the mixture should be equal to the pore volume of the 3DOM ZrTiO₄ support. These precursors were dried at 80°C for 12 h, and the dried precipitate was calcined at 550°C for 4 h at a rate of 1°C/min. Finally, W_xCeMnO₈/3DOM ZrTiO₄ catalysts were obtained, where x means the mass percent of W to ZrTiO₄ support. To obtain single metal oxide supported on 3DOM ZrTiO₄ catalysts, (NH₄)₆H₂W₁₂O₄₀·xH₂O, Ce(NO₃)₃·6H₂O, and Mn(NO₃)₂·4H₂O were individually dissolved in distilled water, and they were added into the ZrTiO₄ support dropwise. Next, the treated processes are similar to those of W_xCeMnO₈/3DOM ZrTiO₄ catalysts. Finally, Mn₂O₃/3DOM ZrTiO₄, CeO₂/3DOM ZrTiO₄, and WO₃/3DOM ZrTiO₄ were obtained.

2.1.3 Synthesis of W₁CeMnO₈/3DOM TiO₂ and W₁CeMnO₈/3DOM ZrO₂ Catalysts

For comparison, W₁CeMnO₈/3DOM TiO₂ and W₁CeMnO₈/3DOM ZrO₂ samples were also prepared by the incipient wetness impregnation method. A similar procedure for the preparation of 3DOM ZrTiO₄ was applied for the preparation of 3DOM TiO₂ and 3DOM ZrO₂ supports. 3DOM TiO₂ and 3DOM ZrO₂ supports were impregnated by the same impregnation solution as that of the W₁CeMnO₈/3DOM ZrTiO₄ catalyst. The obtained precursor was dried at 80°C for 12 h, and after calculation at 550°C for 4 h, W₁CeMnO₈/3DOM TiO₂ and W₁CeMnO₈/3DOM ZrO₂ catalysts were obtained.

2.2 Material Characterization

The phase composition and crystal structure were evaluated by an X-ray diffractometer (Ultima IV, Rigaku) using Cu-K_α radiation as the source with a Ni filter. Nitrogen adsorption–desorption investigation was achieved with a Micromeritics TriStar II: 3020 analyzer to get the textural characteristics of catalysts. The morphology and microstructure of the catalysts were scrutinized by scanning electron microscopy (SEM, Zeiss sigma 500) and transmission electron microscopy (TEM, JEM-F200). Mn 2p, W 4f, Ce 3d, and O 1s binding energies were measured by X-ray photoelectron spectroscopy (XPS, PHI-1600 ESCA). H₂-TPR measurements were conducted using

AutoChemi II2920 equipment; 0.05 g sample was pretreated in N₂ for 1 h at 300°C, followed by cooling down to 25°C. Thereafter, the flow gas was altered to 10-vol% H₂/N₂ with a maximum temperature of 900°C, and the heat treatment rate was kept at 10°C/min; hydrogen consumption was examined using a thermal conductivity detector (TCD). NH₃-TPD was carried out on a conventional flow apparatus, and 0.05 g sample was heated at 600°C in N₂ atmosphere for 1 h and saturated with 1% NH₃ for 1 h. When the temperature cooled to room temperature, N₂ was used to abolish the feebly attached NH₃. At last, the sample was heated to 600°C at a rate of 10°C/min. *In situ* diffuse reflectance infrared Fourier transform (DRIFT) spectroscopy (Thermo Nicolet Is50 spectrometer) was used to investigate the SCR reaction mechanism of the W₁CeMnO₈/3DOM ZrTiO₄ catalyst. The catalyst was first purged with NH₃ or NO + O₂ at 200 and 300°C until adsorption was saturated. Then, the NH₃ or NO + O₂ were closed. After that, the reaction system was purged by N₂, and then, the other corresponding reacted gases were introduced into the *in situ* reaction cell, and the FT-IR spectra were recorded at different times.

2.3 Catalytic Activity Tests

A fixed bed reactor was applied to evaluate the performance of the as-prepared catalysts for the simultaneous elimination of PM and NO_x. The reaction gases comprised 1,000 ppm NH₃, 1,000 ppm NO, and 5% O₂; the balance gas was N₂; and the total flow rate of the gases was 100 ml/min. The catalyst (100 mg) and PM (10 mg) were mixed together, and PM was simulated by Printex-U (Degussa). The reacted gas concentrations (including NH₃, N₂O, NO, NO₂, CO, and CO₂) were tested by the infrared spectrometer. An accurate and reliable quantitative method was established to measure the multiple gaseous components (Qin and Cadet, 1997; Valencia et al., 2009; Sinelli et al., 2010; Stec et al., 2011). The catalytic performance of the oxidation PM was evaluated by the value of T_m, which was defined as the temperature for maximum CO₂ concentration released. The NO reduction was defined by the highest conversion of NO to N₂, and the conversion rate was calculated as follows (Zhang et al., 2011):

$$\text{NO Conversion} = \frac{[\text{NO}]_{\text{inlet}} - [\text{NO}]_{\text{outlet}}}{[\text{NO}]_{\text{inlet}}} \times 100\%,$$

in which [NO]_{inlet} and [NO]_{outlet}, respectively, denote the inlet and outlet concentrations of NO under steady-state conditions.

3 RESULTS AND DISCUSSION

3.1 Activity Tests of the Catalysts

The activities of W_xCeMnO₈/3DOM ZrTiO₄ catalysts for the simultaneous elimination of PM and NO_x were evaluated, and the results are shown in **Figure 1** and **Table 1**. The lower T_m of PM oxidation means high catalytic efficiency, which is important for the design and preparation of catalysts. As shown in **Figure 1A** and **Table 1**, the T_m value of 3DOM ZrTiO₄ support for the removal of PM is 581°C, indicating that the catalytic activity of the support is very weak. Compared with Mn₂O₃/3DOM ZrTiO₄ and

CeO₂/3DOM ZrTiO₄ catalysts, the WO₃/3DOM ZrTiO₄ catalyst has the highest T_m value of 559°C. When W is combined with Ce or Mn, the T_m of the bimetallic supported catalysts decreases. The T_m values of the W₁MnO₈/3DOM ZrTiO₄ and W₁CeO₈/3DOM ZrTiO₄ catalysts are 536 and 558°C, respectively. Interestingly, for the W_xCeMnO₈/3DOM ZrTiO₄ catalysts, the T_m values are all below 500°C. With increasing doping amounts of W, T_m is slightly raised. This indicates that W has a low activity for soot removal, and its activity can be greatly improved by combining with Ce and Mn. Compared with the W₁CeMnO₈/3DOM TiO₂ catalyst, the W₁CeMnO₈/3DOM ZrO₂ catalyst has a lower T_m value of 453°C, and the W₁CeMnO₈/3DOM ZrTiO₄ catalyst has the T_m value of 474°C, which indicates that the catalytic activity can be improved by adding Zr to Ti.

The catalytic performance of NO reduction was evaluated by an operating temperature window (90% NO conversion). As shown in **Figure 1B** and **Table 1**, 3DOM ZrTiO₄ support shows poor performance for NO conversion, and the conversion of over 50% can hardly be obtained on the ZrTiO₄ support. Similarly, the WO₃/ZrTiO₄ catalyst also shows poor NO elimination performance. It is worth noting that the conversion window (90% NO conversion) of the Mn₂O₃/ZrTiO₄ catalyst is only 88°C (157–245°C), and the CeO₂/ZrTiO₄ catalyst has no conversion window over 90%; when W is added to Mn and Ce, respectively, the conversion window of the W₁MnO₈/ZrTiO₄ catalyst has barely changed, but the conversion window of W₁CeO₈/ZrTiO₄ has been greatly improved; the W₁CeMnO₈/ZrTiO₄ catalyst not only exhibits the wide temperature window (250–396°C) but also has high NO conversion, which manifests that the interaction of Ce and W can widen the temperature window, and Mn has the effect of improving the NO conversion. The W_xCeMnO₈/3DOM ZrTiO₄ catalysts exhibit good NO conversion performance except for the W₂CeMnO₈/3DOM ZrTiO₄, indicating that excessive W doping is not beneficial for NO reduction. Compared with W₁CeMnO₈/3DOM ZrTiO₄, W₁CeMnO₈/3DOM TiO₂ and W₁CeMnO₈/3DOM ZrO₂ exhibit low catalytic activity. Therefore, the synergistic effect between Zr and Ti in ZrTiO₄ support indeed has a positive effect to improve the catalytic performance. Based on the above analysis, W₁CeMnO₈/3DOM ZrTiO₄ catalyst not only exhibits the widest temperature window (250–396°C) at a lower temperature for 90% NO conversion but also has the highest NO conversion rate (52%) at the temperature of T_m, which illustrates that the W₁CeMnO₈/ZrTiO₄ catalyst can be considered as one kind of talented catalysts for the simultaneous elimination of soot particles and nitrogen oxides.

3.2 XRD Analysis

The crystal structures of the as-prepared 3DOM ZrTiO₄ support and it-supported catalysts were characterized by XRD measurements, and the results are exhibited in **Figure 2**. As shown in **Figure 2**, the main characteristic peaks at 2θ = 24.75°, 30.51°, 32.82°, 35.66°, 50.27°, and 52.98° can be assigned to the (110), (111), (020), (002), (202), and (221) crystal faces of ZrTiO₄ support (JCPDS No. 80-1783) (Zhang Y. et al., 2015). The peaks at 2θ = 28.50°, 32.76°, 47.82°, and 56.51° of each sample can be assigned to the (111), (200), (220), and (311) crystal faces of cubic

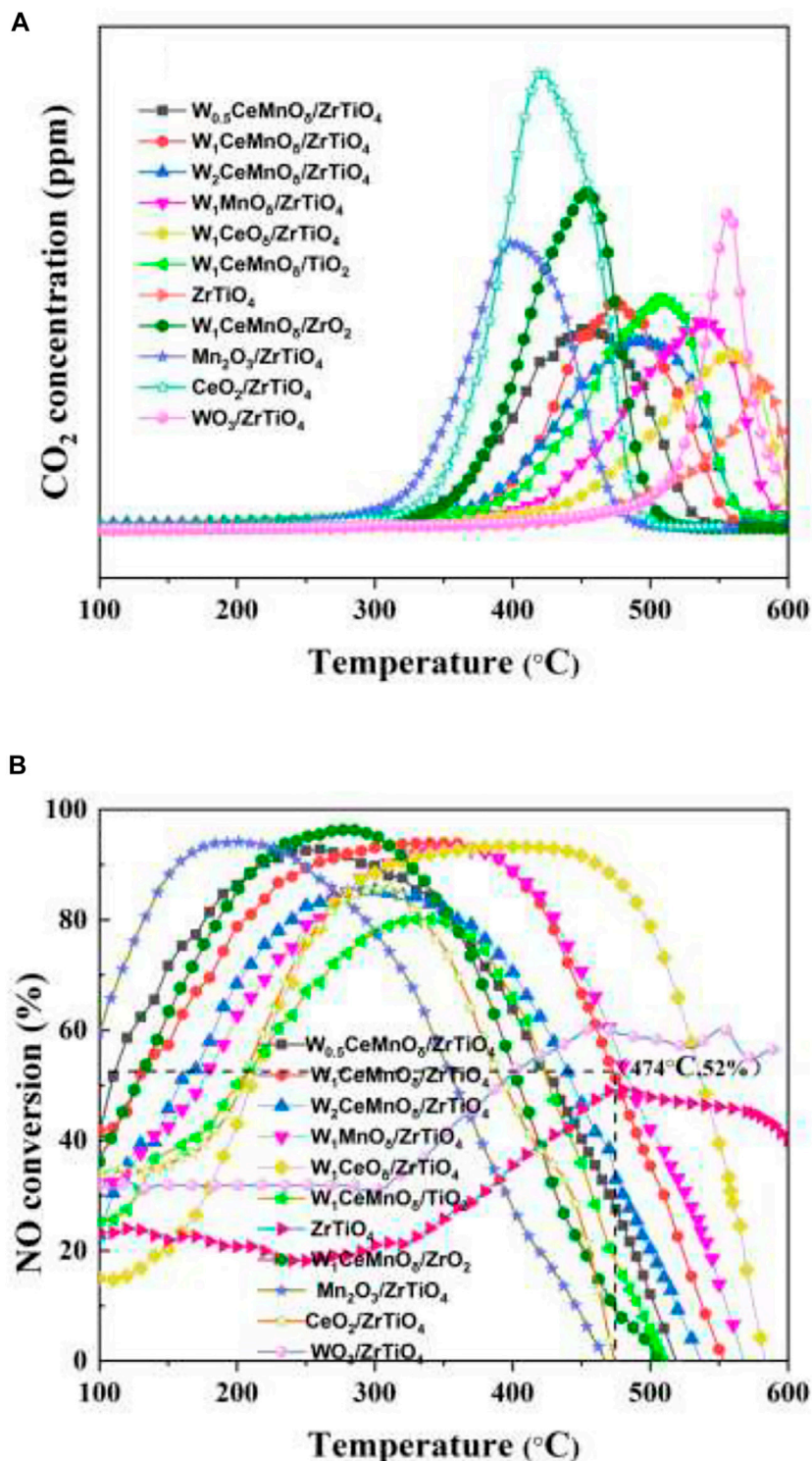


FIGURE 1 | CO₂ concentration cures (A) and NO conversion curves (B) for the simultaneous elimination of PM and NO_x over 3DOM catalysts.

CeO₂ (JCPDS PDF# 43-1002) (Lin et al., 2018). The characteristic peaks of manganese and tungsten oxide cannot be observed because the ionic radius of Mn and W are smaller than that of Ce. Therefore, Mn ions and W ions can easily enter the lattice of

CeO₂. As shown in **Figure 2B**, the diffraction peak of W_xCeMnO₈/3DOM ZrTiO₄ catalysts shifts to a higher angle with respect to the diffraction peak of the CeO₂/3DOM ZrTiO₄ catalyst (i.e., the peak at $2\theta = 28.5^\circ$ shifts to 28.7°),

TABLE 1 | Peak temperature of maximum CO₂ concentration and 90% temperature window of NO conversion over 3DOM catalysts.

Catalysts	T _m ^a /°C	T _{NO,90} ^b /°C
ZrTiO ₄	581	
W ₁ CeMnO ₈ /TiO ₂	504	
W ₁ CeMnO ₈ /ZrO ₂	453	217–323
Mn ₂ O ₃ /ZrTiO ₄	400	157–245
CeO ₂ /ZrTiO ₄	420	
WO ₃ /ZrTiO ₄	559	
W ₁ MnO ₈ /ZrTiO ₄	536	308–394
W ₁ CeO ₈ /ZrTiO ₄	558	313–462
W _{0.5} CeMnO ₈ /ZrTiO ₄	450	220–299
W ₁ CeMnO ₈ /ZrTiO ₄	474	250–396
W ₂ CeMnO ₈ /ZrTiO ₄	492	

^aPeak temperature of maximum CO₂ concentration.

^b90% temperature window of NO conversion.

which confirms the above conclusion. The peaks at $2\theta = 32.95^\circ$, 55.19° , and 23.13° can be assigned to the crystal faces (222), (440), and (211) of α -Mn₂O₃ for Mn₂O₃/3DOM ZrTiO₄ and W₁MnO₈/3DOM ZrTiO₄ catalysts (JCPDS No.41-1442) (Saputra et al., 2014). For the W₁CeMnO₈/3DOM TiO₂ catalyst, the peaks at $2\theta = 25.4^\circ$, 37.9° , 48.1° , 53.9° , 55.2° , and 62.8° belong to anatase TiO₂, in which the crystal faces are (101), (004), (200), (105), (211), and (204), respectively (JCPDS No. 21-1272) (Jiao et al., 2017). For the W₁CeMnO₈/3DOM ZrO₂ catalyst, the peaks at $2\theta = 30.3^\circ$, 35.3° , 50.4° , and 60.2° belong to the characteristic peak of ZrO₂ (JCPDS No. 50-1089). For the WO₃/3DOM ZrTiO₄ catalyst, the peaks at $2\theta = 23.2^\circ$, 23.7° , 24.4° , 28.8° , 34.0° , and 50.2° belong to the characteristic peak of WO₃ (JCPDS No. 20-1323).

3.3 SEM, TEM, and EDS Mapping

The SEM images, as shown in **Figure 3**, demonstrate that all catalysts have highly ordered macropores. From the distributions of macropores' diameters for the as-prepared catalysts in **Figures 3A–I–D–I**, it can be seen that the average diameters of macropores are about 290 ± 20 nm. The diameters of macropores are lower than the PMMA diameter (400 nm), which is related to the shrinkage of polymer templates at high calcination temperature (Cheng et al., 2017a). The skeleton around macropores is constructed by uniform periodically arranged windows (marked with red circles in **Figure 3**), which form the layers through close linkage between the opening windows. Meanwhile, the highly ordered macropores for the as-prepared catalysts indicate the loading process of metal oxides does not destroy 3DOM structures.

TEM and HRTEM images of the W₁CeMnO₈/3DOM ZrTiO₄ catalyst are exhibited in **Figure 4**. **Figure 4A** shows that the W₁CeMnO₈/3DOM ZrTiO₄ catalyst has an ordered macroporous structure and the macropores are linked together by windows layer to layer. This well agrees with the SEM results. Furthermore, the surface of 3DOM ZrTiO₄ is adhered by well-dispersed nanoparticles (NPs), and no large agglomerated particles can be obtained on the 3DOM skeleton, which indicates that metal oxides are evenly distributed on the surface of ZrTiO₄. HRTEM image of W₁CeMnO₈/3DOM ZrTiO₄ is shown in **Figure 4B**; as observed from **Figure 4B**

and the insert images of **Figure 4B**, the lattice fringes with a spacing of 0.32 nm are indexed as (111) planes of CeO₂, and the second lattice fringes with a spacing of 0.36 nm correspond to (011) crystal plane of ZrTiO₄. To study the distribution of W, Ce, Mn, Zr, Ti, and O elements in W₁CeMnO₈/3DOM ZrTiO₄, the HAADF-STEM images and EDS elemental mappings were obtained, and they are shown in **Figure 5**. From **Figures 5B–D**, the elements of O, Ti, and Zr cover the entire 3DOM skeleton because O, Ti, and Zr are the constituent elements of the support. From **Figures 5E, F**, it can be seen that the elements of W, Ce, and Mn are found throughout the surface of the catalyst, even inside the pores.

3.4 BET Study

The N₂ adsorption-desorption isotherms and pore distribution curves of W_xCeMnO₈/3DOM ZrTiO₄ samples are presented in **Figures 6, 7**. The BET data of the as-prepared catalysts are summarized in **Table 2**. As shown in **Figure 6**, all the samples present typical II curves with a nearly linear relationship in the low-pressure vicinity. For 3DOM ZrTiO₄ support, the H3 hysteresis loop increases slowly in the P/P₀ range of 0.4–1.0, which may be due to the scraggly surface of the support. When the active components are loaded on the 3DOM ZrTiO₄ support, the H3 hysteresis loop disappeared in the P/P₀ range of 0.4–0.8 and the intensity in the P/P₀ range of 0.8–1.0 increased sharply. This phenomenon may be due to the scraggly surface of the support being covered by the finely dispersed metal oxide, which makes the surface smooth (Xie et al., 2013).

As shown in **Figure 7**, the as-prepared catalysts exhibit an obvious mesoporous structure. For 3DOM ZrTiO₄ support, the mesopores with a diameter of 2–5 nm belong to the surface gap of the ZrTiO₄ skeleton, and the mesopores with a diameter of 20–35 nm are associated with the accumulation of metal oxide NPs. As shown in **Table 2**, 3DOM ZrTiO₄ exhibits the biggest surface area of 54.0 m²g⁻¹, which may belong to the scraggly surface of ZrTiO₄. However, the surface area decreased when active components are loaded on the ZrTiO₄ support, which may be due to the covering of finely dispersed metal oxide on the scraggly surface. In addition, the surface area of W₁CeMnO₈/3DOM ZrTiO₄ is larger than that of W₁CeMn/3DOM TiO₂ due to the addition of ZrO₂ to TiO₂, which is in accordance with other reports (Zhang et al., 2012; Zhang Y. et al., 2015). Compared with the W₁MnO₈/3DOM ZrTiO₄ catalyst, W₁CeMnO₈/3DOM ZrTiO₄ exhibits a larger surface area, which is attributed to the addition of Ce. The loaded catalysts display a higher total pore volume and average pore size, and this is related to the accumulation effect of active components.

3.5 XPS Analysis

To investigate the valence state of elements and surface composition of the as-prepared catalysts, XPS measurements were carried out, and the results are shown in **Table 3** and **Figure 8**. The ratios of Mn⁴⁺/Mn³⁺, Ce³⁺/Ce⁴⁺, and (O⁻ + O₂⁻)/O²⁻ of W₁CeMnO₈/3DOM ZrTiO₄ are comparatively higher than those of other catalysts, indicating that tungsten, ceria,

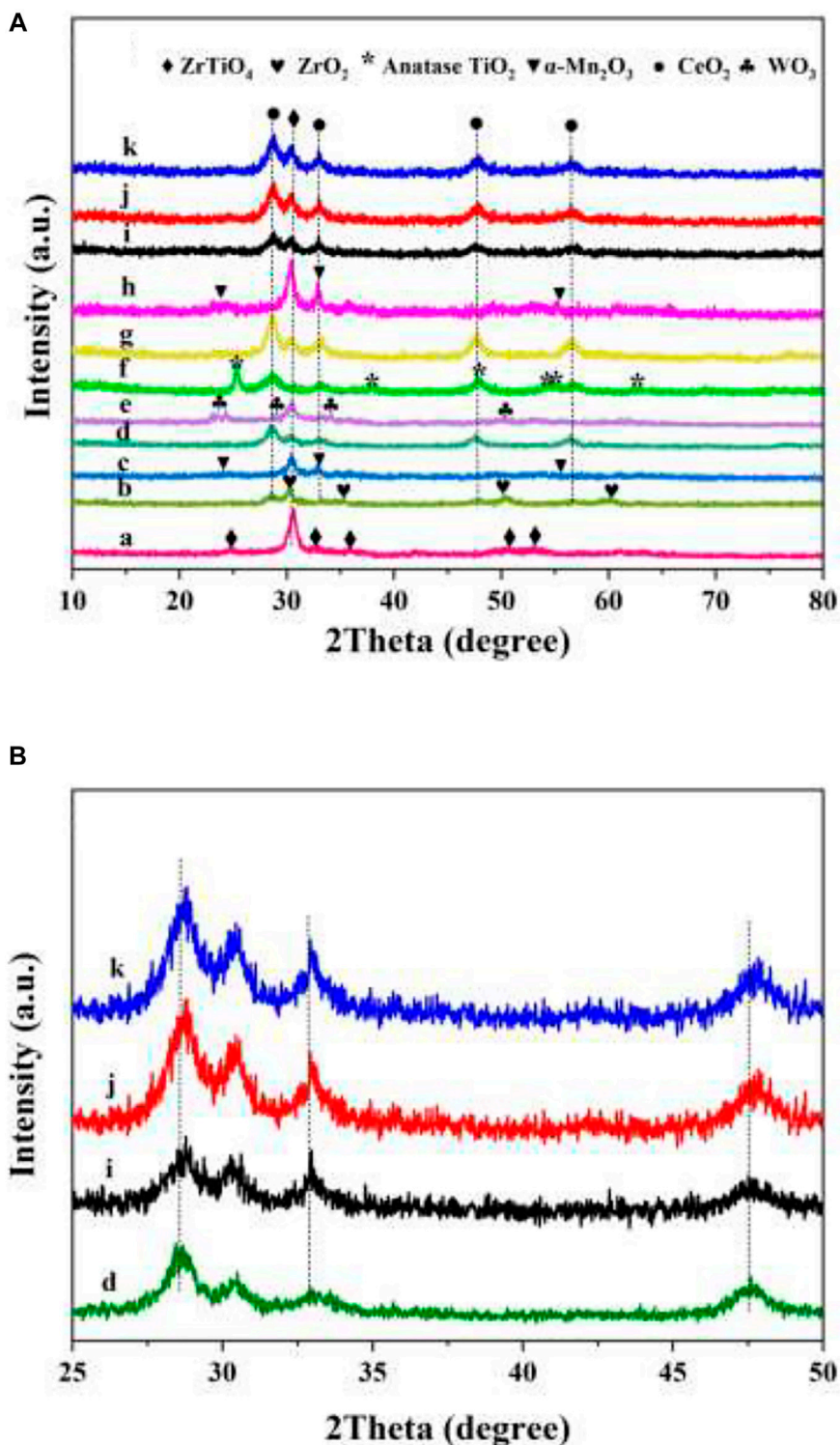


FIGURE 2 | XRD patterns (A) 10–80°, (B) 25–50° of 3DOM materials. (a) ZrTiO₄; (b) W₁CeMnO₈/ZrO₂; (c) Mn₂O₃/ZrTiO₄; (d) CeO₂/ZrTiO₄; (e) WO₃/ZrTiO₄; (f) W₁CeMnO₈/TiO₂; (g) W₁CeO₈/ZrTiO₄; (h) W₁MnO₈/ZrTiO₄; (i) W_{0.5}CeMnO₈/ZrTiO₄; (j) W₁CeMnO₈/ZrTiO₄; (k) W₂CeMnO₈/ZrTiO₄.

manganese, and supports have strong interaction, which leads to the good catalytic performance of the W₁CeMnO₈/3DOM ZrTiO₄ catalyst.

Figure 8A shows the XPS profiles of Mn 2p for the as-prepared catalysts. The spectra of all the catalysts display two peaks. The peaks at 641.2 and 642.9 eV can be assigned to Mn³⁺

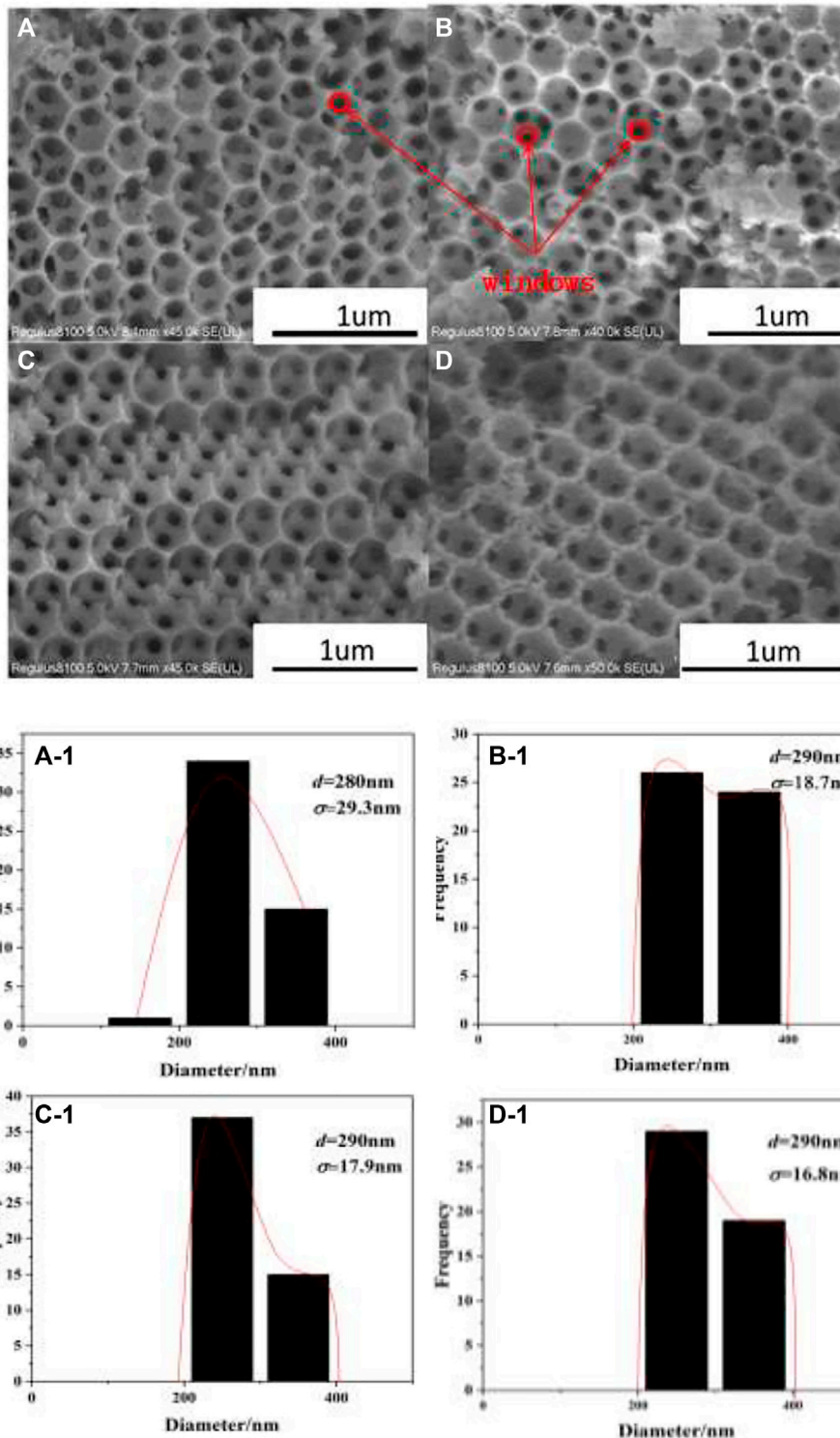
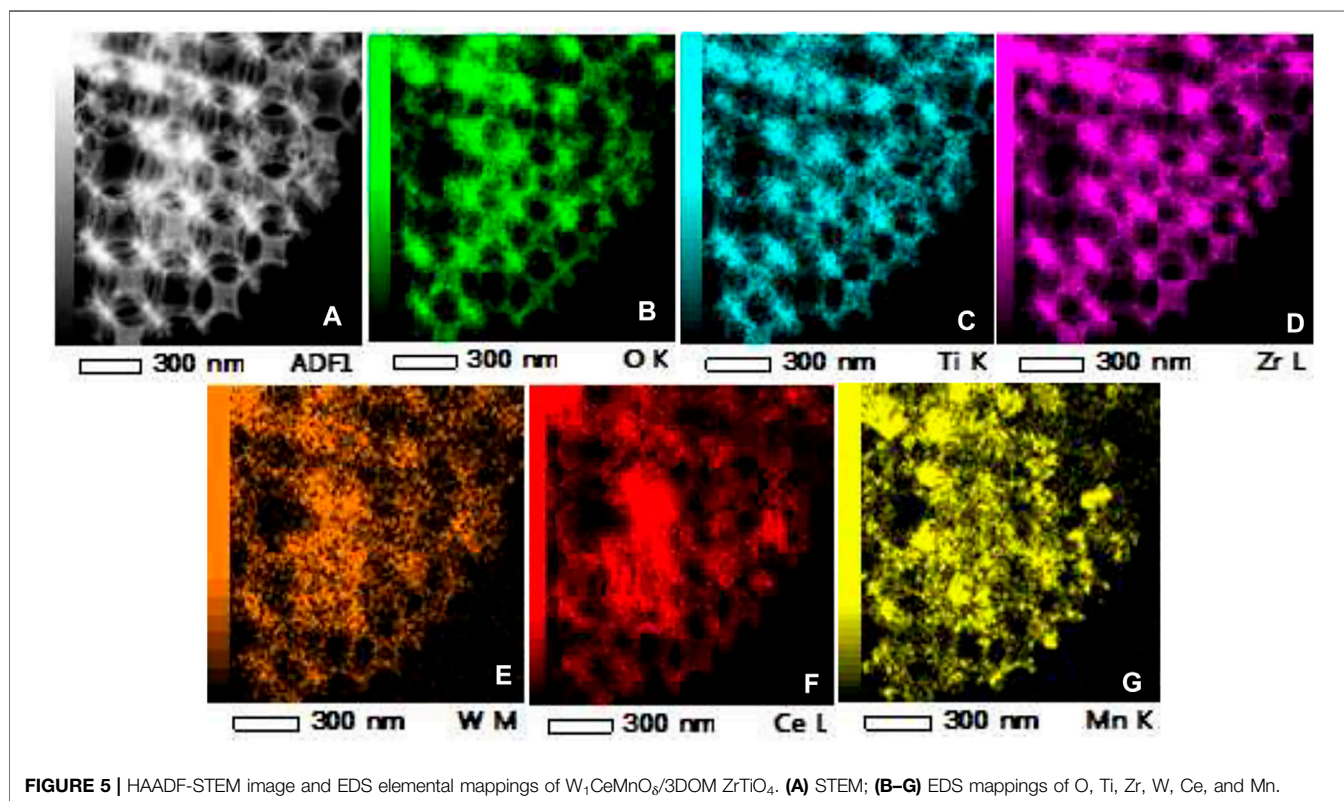
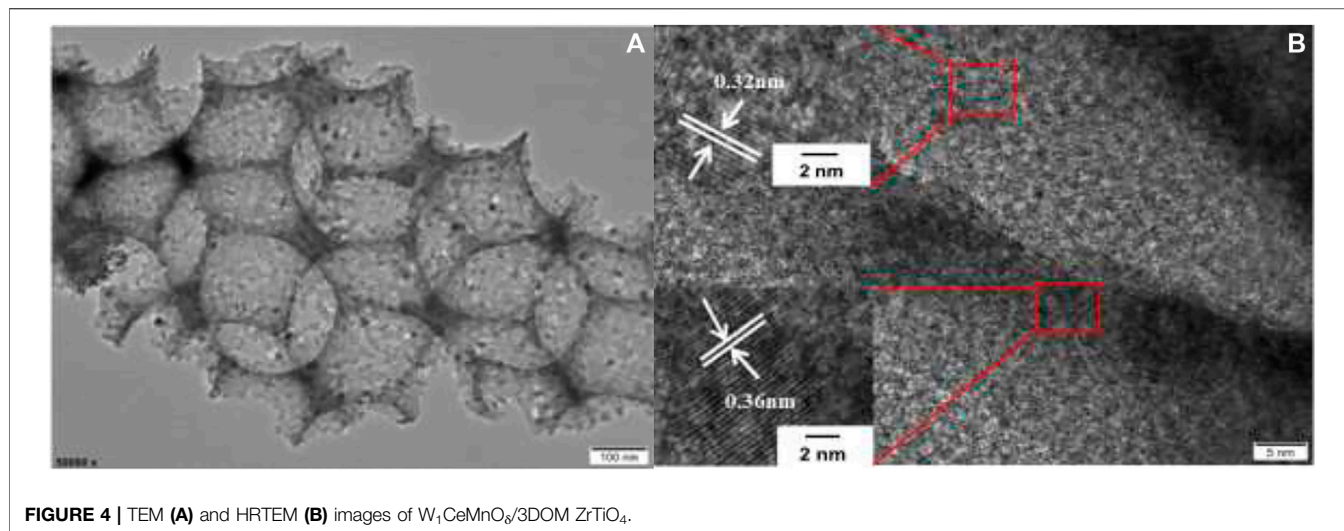


FIGURE 3 | SEM images of 3DOM catalysts and histograms of macropores' diameters. **(A)** W₁CeO₈/ZrTiO₄; **(B)** W₁MnO₈/ZrTiO₄; **(C)** W₁CeMnO₈/ZrTiO₄; **(D)** W₁CeMnO₈/TiO₂.

and Mn⁴⁺ (Li et al., 2016), respectively. It was well known that Mn⁴⁺ species are beneficial for low-temperature SCR (Yao et al., 2019; Li et al., 2021). As shown in **Table 3**, the ratio of Mn⁴⁺/

Mn³⁺ of W₁CeMnO₈/3DOM ZrTiO₄ is higher than that of W₁CeMnO₈/3DOM TiO₂. In addition, the ratio of Mn⁴⁺/Mn³⁺ in the W_xCeMnO₈/3DOM ZrTiO₄ catalysts is higher than that of



the $WMnO_8/3DOM ZrTiO_4$ catalyst, which indicates the strong synergistic effects of Mn and Ce. Ce can accelerate the oxidation of Mn^{3+} to Mn^{4+} , hence, more Mn^{4+} can be produced.

Figure 8B shows the XPS profiles of Ce 3d. The peaks at about 900.5 and 883.5 eV denoted as u' and v' are the major peaks related to the $3d^{10}4f^1$ state of Ce^{3+} ions, and the peaks at about 882.0, 888.8, 897.8, 900.4, 907.1, and 916.2 eV named as v , v'' , v''' , u , u'' , and u''' are related to the $3d^{10}4f^0$ state ascribed to Ce^{4+} (Cheng et al., 2014). According to the peak area ratio of

Ce^{3+} to Ce^{4+} , the content of Ce^{3+} of monometallic oxide CeO_2 is lowest in the as-prepared catalysts, indicating that the support and the doping of other metals can promote the production of more Ce^{3+} . Meanwhile, the content of Ce^{3+} in $W_1CeMnO_8/3DOM ZrTiO_4$ is higher than that of $W_1CeMnO_8/3DOM TiO_2$, which indicates the synergistic effect of Zr and Ti. Similarly, the highest ratio of Ce^{3+}/Ce^{4+} is also found in $W_1CeMnO_8/3DOM ZrTiO_4$, which indicates that the interaction between W and Ce will produce more Ce^{3+} .

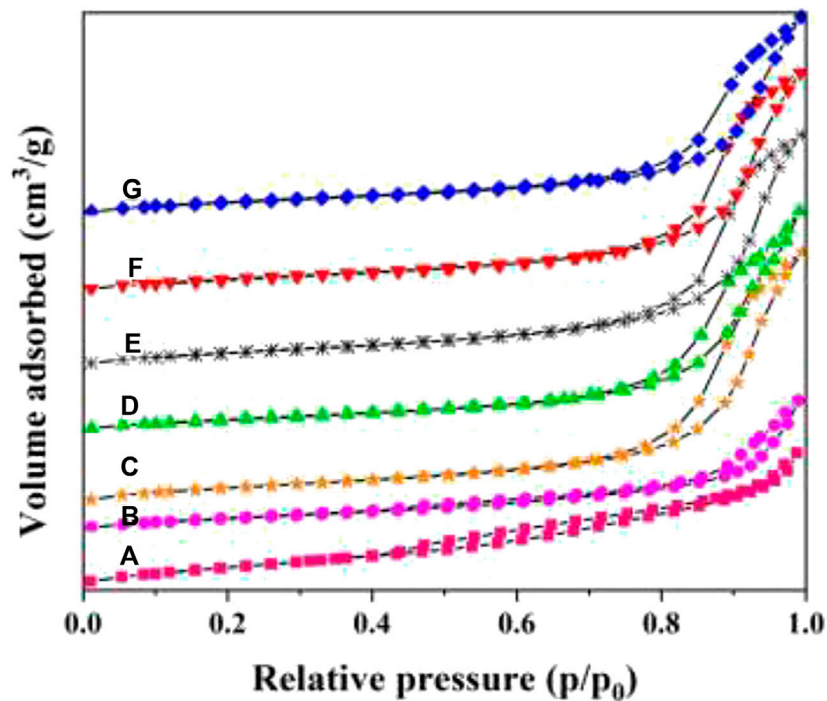


FIGURE 6 | Nitrogen adsorption-desorption isotherms of 3DOM catalysts. (A) ZrTiO₄; (B) W₁MnO₈/ZrTiO₄; (C) W₁CeO₈/ZrTiO₄; (D) W₁CeMnO₈/TiO₂; (E) W_{0.5}CeMnO₈/ZrTiO₄; (F) W₁CeMnO₈/ZrTiO₄; (G) W₂CeMnO₈/ZrTiO₄.

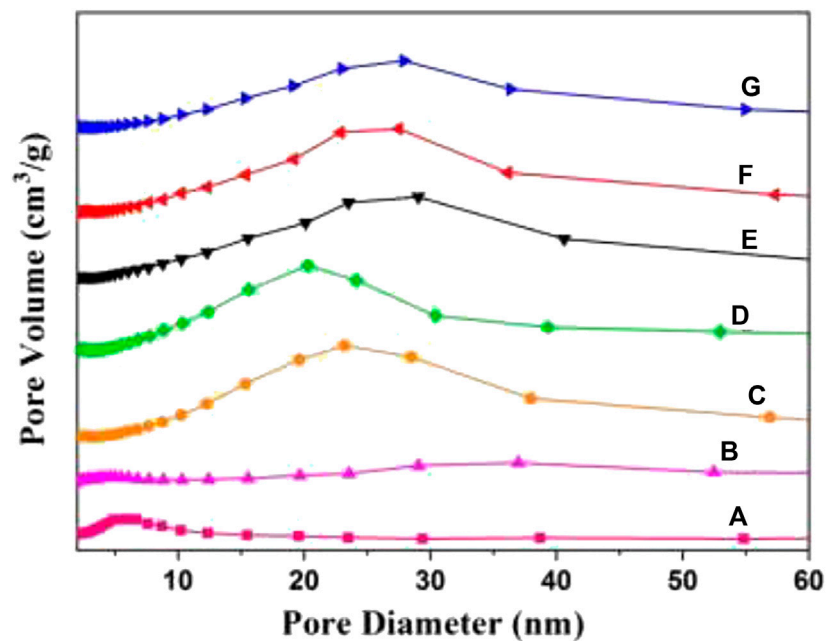


FIGURE 7 | Mesoporous distribution curves of 3DOM catalysts. (A) ZrTiO₄; (B) W₁MnO₈/ZrTiO₄; (C) W₁CeO₈/ZrTiO₄; (D) W₁CeMnO₈/TiO₂; (E) W_{0.5}CeMnO₈/ZrTiO₄; (F) W₁CeMnO₈/ZrTiO₄; (G) W₂CeMnO₈/ZrTiO₄.

TABLE 2 | Textural properties of 3DOM ZrTiO₄ and W_xCeMnO₈/3DOM ZrTiO₄ catalysts.

Catalysts	Surface area (m ² /g) ^a	Total pore volume (cm ³ /g) ^b	Pore size (nm) ^c
ZrTiO ₄	54.0	0.098	6.2
W ₁ MnO ₈ /ZrTiO ₄	37.0	0.095	8.9
W ₁ CeO ₈ /ZrTiO ₄	48.1	0.177	13.7
W ₁ CeMnO ₈ /TiO ₂	40.8	0.155	14.1
W _{0.5} CeMnO ₈ /ZrTiO ₄	44.3	0.163	13.5
W ₁ CeMnO ₈ /ZrTiO ₄	41.2	0.154	13.8
W ₂ CeMnO ₈ /ZrTiO ₄	36.7	0.138	13.7

^aCalculated by the BET method.^bCalculated by BJH desorption cumulative volume of pores between 1.7 and 300 nm diameter.^cCalculated by BJH desorption average pore diameter.**TABLE 3** | XPS result of W_xCeMnO₈/3DOM ZrTiO₄ catalysts.

	Mn ⁴⁺ /Mn ³⁺ (%)	Ce ³⁺ /Ce ⁴⁺ (%)	O _α /O _β (%)
W ₁ MnO ₈ /ZrTiO ₄	44.4		41.7
W ₁ CeO ₈ /ZrTiO ₄		17.2	42.0
W _{0.5} CeMnO ₈ /ZrTiO ₄	60.0	21.1	49.1
W ₁ CeMnO ₈ /ZrTiO ₄	61.1	23.9	51.5
W ₂ CeMnO ₈ /ZrTiO ₄	57.1	13.1	40.1
W ₁ CeMnO ₈ /TiO ₂	49.6	13.6	40.6
Mn ₂ O ₃	57.4		37.8
CeO ₂		12.9	21.3
WO ₃			27.1

Figure 8C gives the W 4f_{5/2} and W 4f_{7/2} peaks at 36.6–37.6 and 34.7–35.7 assigned to W⁶⁺. As shown in **Figure 8C**, W₁CeMnO₈/3DOM ZrTiO₄ has higher binding energy than other catalysts. The higher binding energy generally represents the lower density of electron cloud, as W⁶⁺ has only four coordination bonds with surrounding O-atoms which can generate excess electrons, so Ce⁴⁺ can be substituted by W⁶⁺ and produce one or two excess electrons, and the excess electrons will be compensated by producing one or two Ce³⁺; these Ce³⁺ ions play a crucial role in the generation of oxygen vacancy due to its charge imbalance and unsaturated chemisorption bond; thus, it further enhances the catalytic activity greatly (Liu et al., 2020).

As shown in **Figure 8D**, O 1s peaks are fitted into two peaks at 528.0–530.0 and 530.0–532.0 eV (according to Gaussian bands), and those peaks are ascribed to lattice oxygen (O²⁻, denoted as O_β) and chemically adsorbed oxygen (O₂⁻ and/or O⁻, denoted as O_α), respectively (Zhang S. et al., 2015). Generally speaking, O_α is active oxygen species that has higher mobility than lattice oxygen, and it is the determining factor for low-temperature NH₃-SCR reaction and soot oxidation. Because gas-phase NO is more easily obtained and reacts with active oxygen species and forms NO₂, NO₂ will react with NO and NH₃ in the fast-SCR mode and react with soot directly. Hence, the rates for NH₃-SCR and soot oxidation reactions were enhanced. Based on the results in **Table 3** and **Figure 1**, the O_α/O_β ratio of monometallic oxide Mn₂O₃, CeO₂, and WO₃ is lower than that of other as-prepared catalysts, which manifest the effect of supports and other doping metals. W₁CeMnO₈/3DOM ZrTiO₄ has the highest O_α/O_β ratio of 51.5% among the as-prepared catalysts and shows the highest NO conversion rate at temperature

T_m. Therefore, the high ratio of O_α/O_β plays an important role in the simultaneous catalytic elimination of PM and NO_x.

3.6 H₂-TPR

Catalysts with excellent redox properties are required in the simultaneous removal reaction. H₂-TPR is usually applied for measuring the redox ability of catalysts. **Figure 9** gives the H₂-TPR results of the as-prepared catalysts. As shown in **Figure 9A**, the 3DOM ZrTiO₄ support has almost no reduction peak, indicating that the redox capacity of the support is very weak. CeO₂/3DOM ZrTiO₄ has one reduction peak at 618°C, which is related to the reduction of surface oxygen species of ceria (Ma et al., 2012), since the reduction of bulk ceria occurred only above 750°C (Andreeva et al., 2004; Ndifor et al., 2007). When W is added into CeO₂/3DOM ZrTiO₄, the shoulder peak at 618°C belongs to the reduction of surface CeO₂, and the peaks at 695°C are assigned to the reduction of surface WO_x (Ma et al., 2012). When Mn is doped into CeO₂/ZrTiO₄, three reduction peaks can be obtained. The first peak at 365°C is associated with the reduction of MnO₂ to Mn₂O₃, the peak at 465°C is related to the reduction of surface Mn₂O₃ to Mn₃O₄, and the third shoulder peak at 531°C belongs to the reduction of surface Mn₃O₄ to MnO (Yu et al., 2014).

As shown in **Figure 9E**, W₁CeMnO₈/3DOM TiO₂ displays one reduction peak at 490°C, which belongs to the overlapped reduction of surface oxygen. For W_xCeMnO₈/3DOM ZrTiO₄ catalysts, the TPR curves display two broad peaks, the former can belong to the reductions of the MnO₂ to Mn₂O₃ and Mn₂O₃ to Mn₃O₄, and the latter may be related to the reductions of Mn₃O₄ to MnO, CeO₂ to Ce₂O₃, and WO_x to W. Among the W_xCeMnO₈/3DOM ZrTiO₄ catalysts, the peaks of the W₁CeMnO₈/3DOM ZrTiO₄ catalyst shift to lower temperatures and the peak in the lower temperature has a wider reduction peak area, indicating that the 3DOM W₁CeMnO₈/3DOM ZrTiO₄ catalyst has strong reduction ability and much Mn⁴⁺ species. The Mn⁴⁺/Mn³⁺ ionic couple have proper redox characteristics and easily deliver more active sites for improving activity; therefore, the W₁CeMnO₈/3DOM ZrTiO₄ catalyst shows good simultaneous removal activity.

3.7 NH₃-TPD

Surface acidity plays a significant role in NH₃-SCR reaction (Xu et al., 2016; Xu et al., 2017). NH₃-TPD was used to evaluate the

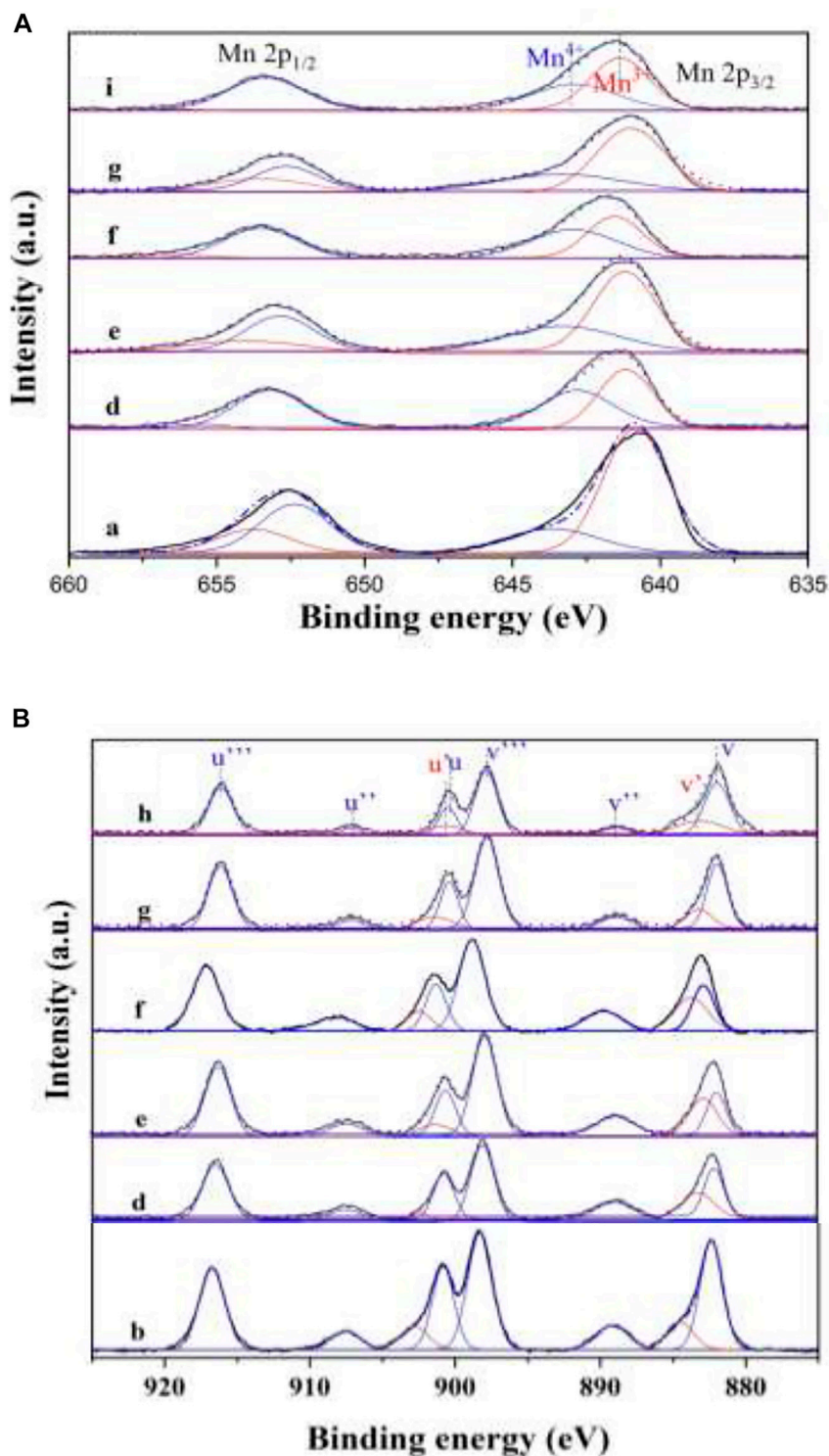


FIGURE 8 | XPS spectra of Mn 2p (A), Ce 3d (B), W 4f (C), and O 1s (D). (a) Mn₂O₃; (b) CeO₂; (c) WO₃; (d) W₁CeMnO₈/TiO₂; (e) W_{0.5}CeMnO₈/ZrTiO₄; (f) W₁CeMnO₈/ZrTiO₄; (g) W₂CeMnO₈/ZrTiO₄; (h) W₁CeO₈/ZrTiO₄; (i) W₁MnO₈/ZrTiO₄.

amount and strength of surface acid sites. Therefore, the NH₃-TPD profiles of the as-prepared catalysts were tested, and the results are shown in **Figure 10**. All the catalysts have broad peaks

in the temperature range of 50–350°C, which is related to the desorption of NH₃ on the weak and medium acid sites. Interestingly, these peaks are nearly at the same location, and

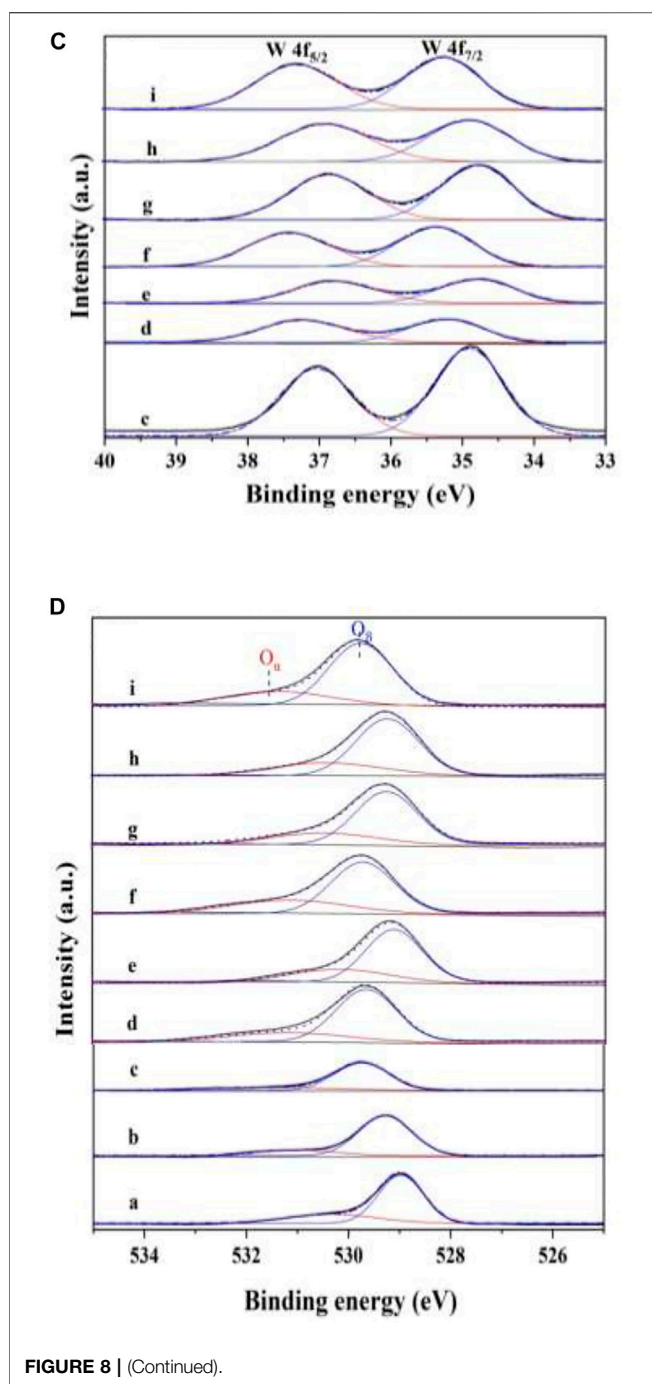


FIGURE 8 | (Continued).

no significant difference can be observed. Compared with the W₁CeMnO₈/3DOM TiO₂ catalyst, the peak area of the W₁CeMnO₈/3DOM ZrTiO₄ catalyst is larger, which indicates that the W₁CeMnO₈/3DOM ZrTiO₄ catalyst has more acid sites due to the doping of Zr in the ZrTiO₄ support. In comparison with W₁MnO₈/3DOM ZrTiO₄ catalyst, more acid sites can be seen in W₁CeMnO₈/3DOM ZrTiO₄, and these acid sites may come from the electron-unsaturated W⁶⁺, as W⁶⁺ enter the CeO₂ lattice, leading to lower coordination between W⁶⁺ and surrounding oxygen, so it needs to share more electrons to

balance the charge transfer. Therefore, the above analyses verify the experimental results that the W₁CeMnO₈/3DOM ZrTiO₄ catalyst has the highest NO removal activity.

4 DISCUSSIONS

4.1 Effects of 3DOM Structure on Catalytic Performances

Soot combustion is the reaction of gas–solid–solid, and the contact efficiency between catalyst and soot is a significant factor for controlling the catalytic activity. 3DOM catalysts have highly ordered macroporous structures with diameter higher than 100 nm (SEM results). Because the diameter of soot particles (≈25 nm) is smaller than that of macropores, the large pores can capture soot particles and transfer soot particles to the inner active sites so that the active sites of catalysts can be fully utilized. Meanwhile, the diffusion resistance is reduced due to highly ordered macropores. Some previous work also confirmed the effect of the macroporous structure on improving catalytic activity (Yu et al., 2019; Yu X. et al., 2021).

In addition, the effects of NPs also play important roles in removing soot particles, such as the quantum size effects and surface effects. In this work, the active components are formed nanoparticles on the surface of 3DOM ZrTiO₄ support. From the TEM results, it can be found that the diameter of active components is well falling into the scale of NPs. At the same time, gaseous reactants are more easily absorbed due to a lot of NPs on the surface of 3DOM ZrTiO₄ supports, thus improving the efficiency of the catalytic reaction.

4.2 Possible Reaction Mechanism for Simultaneous deSoot and deNO_x

To more deeply understand the reaction essence of simultaneous deSoot and deNO_x, according to the results in this work and previous reports, the possible reaction mechanisms are also speculated and described in Scheme 1.

For the reaction of deSoot, based on the results of XPS (Figure 8) and H₂-TPR (Figure 9), the 3DOM W₁CeMnO₈/3DOM ZrTiO₄ catalyst has more Mn⁴⁺, Ce³⁺, and O_α than other as-prepared catalysts, which indicates that it has more active sites, so gas-phase O₂ molecules are more easily to be adsorbed and activated on the active sites (oxygen vacancies). On the one hand, adsorbed O₂ forms active oxygen species, then soot traps the active oxygen species and forms surface oxygen–carbon complexes (SOC), and finally, the SOC further decomposes and produces CO₂ and CO. On the other hand, these active oxygen species react with NO to form NO₂; NO₂ has stronger oxidation capacity than active oxygen species, so it can react with soot directly and changes the reaction path from gas–solid–solid to gas–gas–solid, thus accelerating the process of soot combustion. Therefore, the W₁CeMnO₈/3DOM ZrTiO₄ catalyst has a lower T_m value of 474°C (Figure 1).

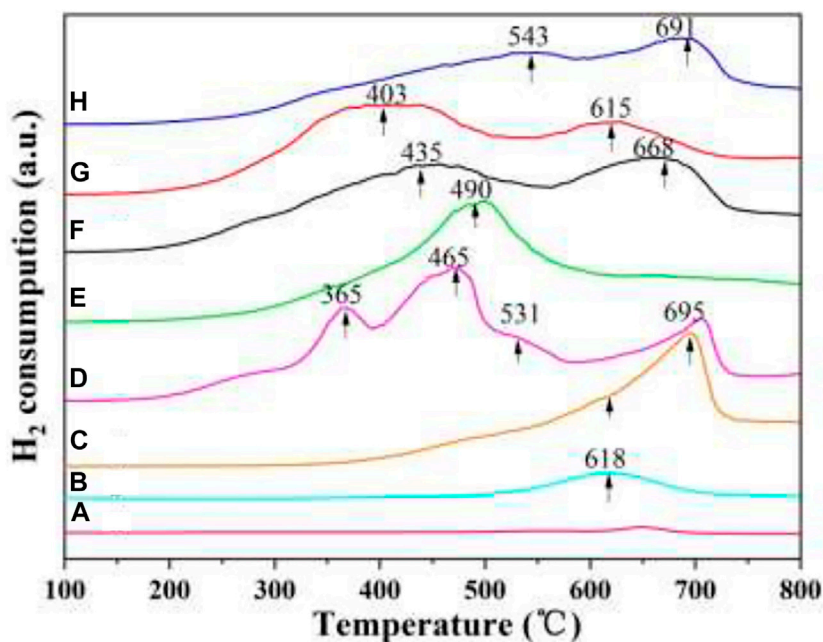


FIGURE 9 | H₂-TPR profiles of the 3DOM catalysts. (A) ZrTiO₄; (B) CeO₂/ZrTiO₄; (C) W₁CeO₈/ZrTiO₄; (D) W₁MnO₈/ZrTiO₄; (E) W₁CeMnO₈/TiO₂; (F) W_{0.5}CeMnO₈/ZrTiO₄; (G) W₁CeMnO₈/ZrTiO₄; (H) W₂CeMnO₈/ZrTiO₄.

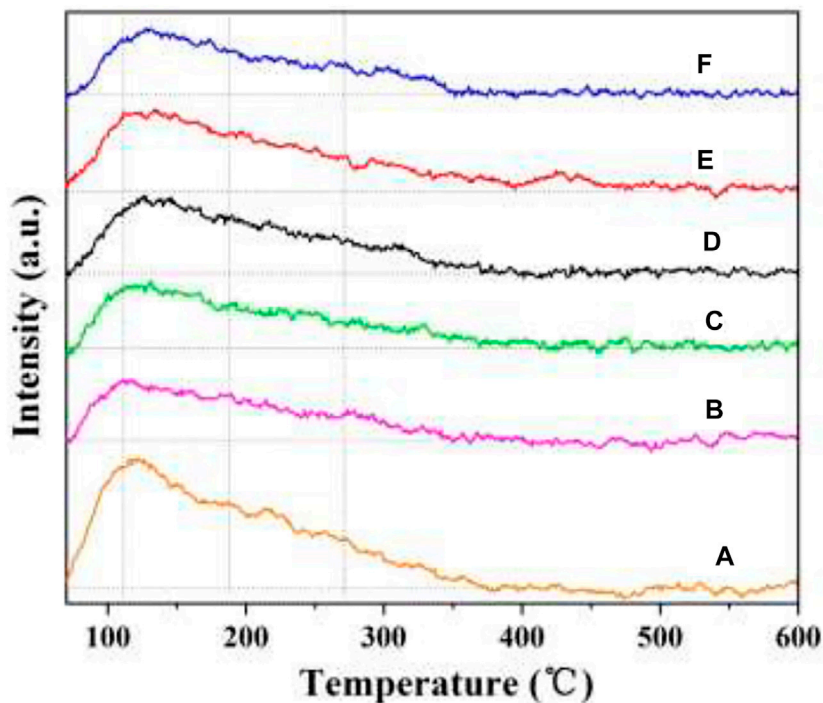


FIGURE 10 | NH₃-TPD profiles of the 3DOM catalysts. (A) W₁CeO₈/ZrTiO₄; (B) W₁MnO₈/ZrTiO₄; (C) W₁CeMnO₈/TiO₂; (D) W_{0.5}CeMnO₈/ZrTiO₄; (E) W₁CeMnO₈/ZrTiO₄; (F) W₂CeMnO₈/ZrTiO₄.

For the reaction of deNO_x, in order to investigate the SCR reaction mechanism of the W₁CeMnO₈/3DOM ZrTiO₄ catalyst, *in situ* DRIFTS were measured at 200 and 300°C, and the results

are shown in **Figure 11**. As shown in **Figure 11A**, after being purged by N₂, several absorbance bands were observed. The bands centered at 1,198 and 1,633 cm⁻¹ are ascribed to

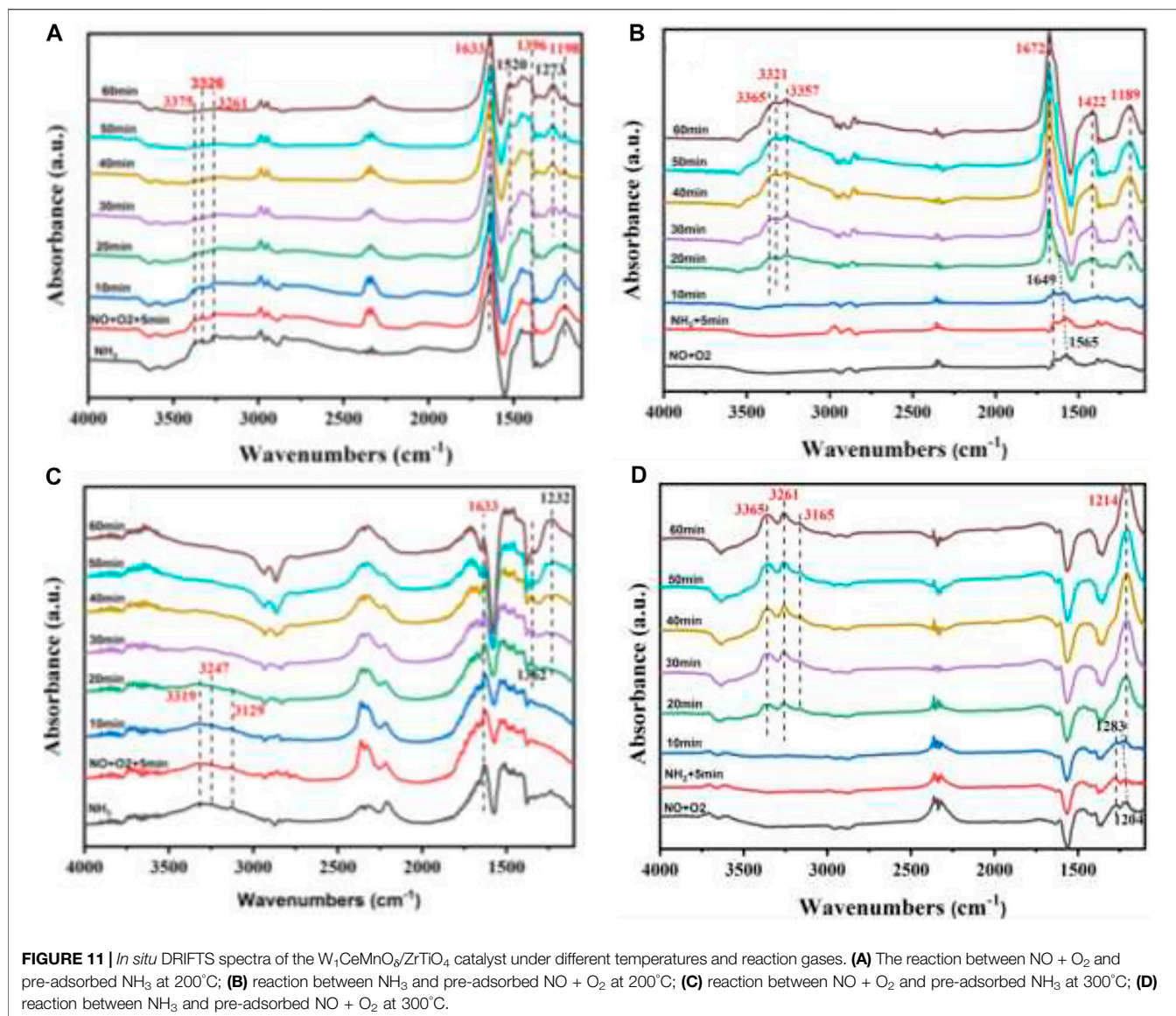
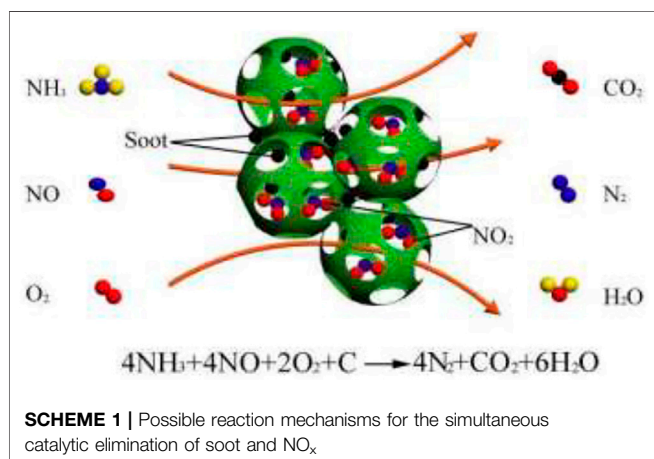


FIGURE 11 | *In situ* DRIFTS spectra of the $W_1CeMnO_6/ZrTiO_4$ catalyst under different temperatures and reaction gases. **(A)** The reaction between $NO + O_2$ and pre-adsorbed NH_3 at $200^\circ C$; **(B)** reaction between NH_3 and pre-adsorbed $NO + O_2$ at $200^\circ C$; **(C)** reaction between $NO + O_2$ and pre-adsorbed NH_3 at $300^\circ C$; **(D)** reaction between NH_3 and pre-adsorbed $NO + O_2$ at $300^\circ C$.



adsorbed NH_3 on Lewis acidic sites, and the bands at $1,396\text{ cm}^{-1}$ belong to the coordinated NH_4^+ on Bronsted acid sites, while the bands at $3,100\text{--}3,500\text{ cm}^{-1}$ are attributed to N-H stretching vibration of coordinated ammonia (Tan et al., 2018; Liu et al., 2020). When $NO + O_2$ was introduced into the *in situ* reaction cell, all the bands belonging to the ammonia species are reduced gradually in their intensities with increasing time, and the IR bands ($1,198$ and $3,100\text{--}3,500\text{ cm}^{-1}$) disappear after 20 min. At the same time, the nitrate species including bidentate nitrate ($1,273\text{ cm}^{-1}$) and monodentate nitrate ($1,520\text{ cm}^{-1}$) begin to appear on the surface of the catalyst, including bidentate nitrate ($1,273\text{ cm}^{-1}$) and monodentate nitrate ($1,520\text{ cm}^{-1}$). These results indicate that the gas phase NO reacts with the coordinated NH_3 on the surface of the $W_1CeMnO_6/3DOM\ ZrTiO_4$ catalyst through the E-R mechanism.

As shown in **Figure 11B**, after being purged by N₂, bidentate nitrates (1,565 cm⁻¹) and bridging nitrates (1,649 cm⁻¹) (Liu et al., 2020; Wang et al., 2020) were formed on the surface of the W₁CeMnO₈/3DOM ZrTiO₄ catalyst because the mixture of NO + O₂ was adsorbed on the surface of the catalyst. When NH₃ was introduced into the *in situ* reaction cell, the bands related to nitrate species decreased gradually in the first 10 min, and no adsorption peaks were found for NH₃ species, indicating that the gas phase NH₃ reacts with the nitrate species. After 20 min, the bands belonging to NH₃ species begin to appear, indicating the existence of ammonia on the surface of the catalyst; the bands at 1,189 and 1,672 cm⁻¹ belong to the adsorbed NH₃ on Lewis acidic sites; the bands at 1,422 cm⁻¹ belong to the coordinated NH₃⁺ on Bronsted acid sites; and the peaks at 3,100–3,500 cm⁻¹ belong to N-H stretching vibration of coordinated ammonia. Interestingly, the bands at 1,565 cm⁻¹ (bidentate nitrates) begin to shift after 5 min and decrease slowly within 15 min. After 15 min, the peak at 1,565 cm⁻¹ (bidentate nitrates) disappeared and the peak belonged to the NH₃ species increased gradually, so the IR band at 1,672 cm⁻¹ may be caused by the overlap of the bidentate nitrates (1,565 cm⁻¹), bridging nitrates (1,649 cm⁻¹), and the coordinated NH₃ adsorbed on the Lewis acid site (1,672 cm⁻¹). Based on the above results and discussion, it can be found that bidentate nitrate (1,565 cm⁻¹) and active NH₃ can coexist on the surface of the W₁CeMnO₈/3DOM ZrTiO₄ catalyst and the SCR reaction mechanism of the W₁CeMnO₈/3DOM ZrTiO₄ catalyst can be both E-R mechanism and L-H mechanism at 200°C.

Figures 11C, D show the *in situ* DRIFT spectra of the W₁CeMnO₈/3DOM ZrTiO₄ catalyst measured at 300°C. As shown in **Figure 11C**, similarly, the catalyst was first treated by NH₃. After being purged by N₂, the bands centered at 1,633 cm⁻¹ are ascribed to the adsorbed NH₃ on Lewis acidic sites, and the bands at 3,100–3,500 cm⁻¹ are attributed to N-H stretching vibration of coordinated ammonia. When NO + O₂ was introduced into the *in situ* reaction cell, the intensities of all the bands belonging to the ammonia species gradually reduced, and the IR bands (3,100–3,500 cm⁻¹) disappeared after 20 min. The bands, which belong to nitrate species, appear; the band centered at 1,232 cm⁻¹ is ascribed to bridging nitrate; and the band at 1,362 cm⁻¹ is attributed to bidentate nitrate. These results indicate that gas phase NO reacts with coordinated NH₃ also through the E-R mechanism at 300°C.

As shown in **Figure 11D**, the catalyst was first treated with NO + O₂. After purging with N₂, the bands assigned to bridging nitrates (1,204 cm⁻¹) and monodentate nitrates (1,283 cm⁻¹) were detected to demonstrate the formation of these nitrate species on the surface of the catalyst. When NH₃ was introduced, the band intensity related to nitrate species decreased gradually in the first 10 min, and no adsorption peaks were found for NH₃ species. After 20 min, several bands began to appear; the bands at 1,214 cm⁻¹ are ascribed to adsorbed NH₃ on Lewis acidic sites, and the bands at 3,100–3,500 cm⁻¹ are attributed to N-H stretching vibrational

of coordinated ammonia. Similar to the case at 200°C, the bands at 1,204 cm⁻¹ were shifted after 5 min and band intensity decreased slowly. After 15 min, the peaks at 1,204 and 1,283 cm⁻¹ disappeared, and the intensity of the peak belonging to the NH₃ species was increased gradually. The IR band at 1,214 cm⁻¹ may be the overlap of the bridging nitrates (1,204 cm⁻¹), monodentate nitrates (1,283 cm⁻¹), and the adsorbed NH₃ species. These results indicate that the reaction at 300°C is similar to the reaction at 200°C.

To sum up, the reaction mechanism for the simultaneous deSoot and deNO_x is a complex mechanism that mixes two reactions together. In this work, four mechanisms, including the active oxygen mechanism, NO₂-assisted mechanism, L-H mechanism, and E-R mechanism, were proposed, and these four mechanisms work together in the simultaneous elimination reaction.

5 CONCLUSION

3DOM ZrTiO₄ support and a series of W_xCeMnO₈/3DOM ZrTiO₄ oxide catalysts were fabricated by the colloidal crystal template method and applied to the simultaneous elimination of PM and NO_x. Based on the analyses of characterization and activity evaluation results, the as-prepared catalysts have a high-quality 3DOM structure, and the W₁CeMnO₈/3DOM ZrTiO₄ catalyst exhibits the best catalytic performance due to the perfect structure, large surface area, abundant acid sites, and the synergistic effect among the active components. Among the as-prepared catalysts, W₁CeMnO₈/3DOM ZrTiO₄ exhibits the widest temperature window (250–396°C) at a lower temperature for 90% NO conversion but also has the highest NO conversion rate (52%) at the temperature of T_m for soot combustion. The catalytic mechanism for the simultaneous elimination of soot particulate matter and nitrogen oxides over W₁CeMnO₈/3DOM ZrTiO₄ catalyst is mainly governed *via* the active oxygen mechanism, NO₂-assisted mechanism, L-H mechanism, and E-R mechanism. The as-prepared W_xCeMnO₈/3DOM ZrTiO₄ catalysts have application prospects for the simultaneous elimination of soot particulate matter and nitrogen oxides from diesel engine exhausts, owing to easy preparation, low cost, and high catalytic activity.

DATA AVAILABILITY STATEMENT

The original contributions presented in the study are included in the article/Supplementary Material, further inquiries can be directed to the corresponding authors.

AUTHOR CONTRIBUTIONS

RW conducted the catalyst preparation and wrote the manuscript. CZ and DL performed the activity test and

characterization. ZS, AK, YW, and JL discussed the mechanism part. XY and ZZ conceived the project and improved the text.

FUNDING

This work was supported by the Key Research and Development Program of MOST (2017YFE0131200), the National Natural Science Foundation of China (U1908204, 22072095, and 21761162016), the University Joint Education Project for

China-Central and Eastern European Countries (2021097), the National Engineering Laboratory for Mobile Source Emission Control Technology (NELMS 2018A04), Education Office of Liaoning Province (LJC202004 and LJC202005), the University level innovation team of Shenyang Normal University, Major Incubation Program of Shenyang Normal University (ZD201901), and the National Centre for Research and Development, Poland, grant PNOX no. WPC1/PNOX/2019 (MOST program).

REFERENCES

- Andreeva, D., Nedyalkova, R., Ilieva, L., and Abrashev, M. V. (2004). Gold-vanadia Catalysts Supported on Ceria-Alumina for Complete Benzene Oxidation. *Appl. Catal. B: Environ.* 52, 157–165. doi:10.1016/j.apcatb.2004.03.019
- Bueno-López, A., Lozano-Castelló, D., and Anderson, J. A. (2016). NOx Storage and Reduction over Copper-Based Catalysts. Part 1: BaO + CeO₂ Supports. *Appl. Catal. B: Environ.* 198, 189–199. doi:10.1016/j.apcatb.2016.05.067
- Chen, B., Liu, Y., Chen, S., Zhao, X., Yue, W., and Pan, X. (2016). Nitrogen-rich Core/shell Magnetic Nanostructures for Selective Adsorption and Separation of Anionic Dyes from Aqueous Solution. *Environ. Sci. Nano* 3, 670–681. doi:10.1039/c6en00022c
- Chen, M., Wang, L., Yu, X., and Zhao, Z. (2019). Application of Mn-Based Catalysts for the Catalytic Combustion of Diesel Soot. *Prog. Chem.* 31, 723–737.
- Cheng, K., Liu, J., Zhang, T., Li, J., Zhao, Z., Wei, Y., et al. (2014). Effect of Ce Doping of TiO₂ Support on NH₃-SCR Activity over V₂O₅-WO₃/CeO₂-TiO₂ Catalyst. *J. Environ. Sci.* 26, 2106–2113. doi:10.1016/j.jes.2014.08.010
- Cheng, Y., Liu, J., Zhao, Z., Wei, Y., Song, W., and Xu, C. (2017a). The Simultaneous Purification of PM and NOx in Diesel Engine Exhausts over a Single 3DOM Ce_{0.9}-xFe_{0.1}ZrxO₂ Catalyst. *Environ. Sci. Nano* 4, 1168–1177. doi:10.1039/c7en00170c
- Cheng, Y., Song, W., Liu, J., Zheng, H., Zhao, Z., Xu, C., et al. (2017b). Simultaneous NOx and Particulate Matter Removal from Diesel Exhaust by Hierarchical Fe-Doped Ce-Zr Oxide. *ACS Catal.* 7, 3883–3892. doi:10.1021/acscatal.6b03387
- Choi, B., and Lee, K.-S. (2014). LNT/CDPF Catalysts for Simultaneous Removal of NOx and PM from Diesel Vehicle Exhaust. *Chem. Eng. J.* 240, 476–486. doi:10.1016/j.cej.2013.10.100
- Dai, Y., Yao, J., Song, Y., Wang, S., and Yuan, Y. (2016). Enhanced Adsorption and Degradation of Phenolic Pollutants in Water by Carbon Nanotube Modified Laccase-Carrying Electrospun Fibrous Membranes. *Environ. Sci. Nano* 3, 857–868. doi:10.1039/c6en00148c
- Epling, W. S., Campbell, L. E., Yezerets, A., Currier, N. W., and Parks, J. E. (2004). Overview of the Fundamental Reactions and Degradation Mechanisms of NOx Storage/Reduction Catalysts. *Catal. Rev.* 46, 163–245. doi:10.1081/cr-200031932
- Fritz, A., and Pitchon, V. (1997). The Current State of Research on Automotive Lean NOx Catalysis. *Appl. Catal. B: Environ.* 13, 1–25. doi:10.1016/s0926-3373(96)00102-6
- Gogos, A., Kaegi, R., Zenobi, R., and Bucheli, T. D. (2014). Capabilities of Asymmetric Flow Field-Flow Fractionation Coupled to Multi-Angle Light Scattering to Detect Carbon Nanotubes in Soot and Soil. *Environ. Sci. Nano* 1, 584–594. doi:10.1039/c4en00070f
- Jiao, J., Wei, Y., Zhao, Y., Zhao, Z., Duan, A., Liu, J., et al. (2017). AuPd/3DOM-TiO₂ Catalysts for Photocatalytic Reduction of CO₂: High Efficient Separation of Photogenerated Charge Carriers. *Appl. Catal. B: Environ.* 209, 228–239. doi:10.1016/j.apcatb.2017.02.076
- Jin, R., Liu, Y., Wang, Y., Cen, W., Wu, Z., Wang, H., et al. (2014). The Role of Cerium in the Improved SO₂ Tolerance for NO Reduction with NH₃ over Mn-Ce/TiO₂ Catalyst at Low Temperature. *Appl. Catal. B: Environ.* 148–149, 582–588. doi:10.1016/j.apcatb.2013.09.016
- Li, H., Wu, S., Wu, C.-Y., Wang, J., Li, L., and Shih, K. (2015). SCR Atmosphere Induced Reduction of Oxidized Mercury over CuO-CeO₂/TiO₂ Catalyst. *Environ. Sci. Technol.* 49, 7373–7379. doi:10.1021/acs.est.5b01104
- Li, Q., Meng, M., Dai, F., Zha, Y., Xie, Y., Hu, T., et al. (2012). Multifunctional Hydrotalcite-Derived K/MnMgAlO Catalysts Used for Soot Combustion, NOx Storage and Simultaneous Soot-NOx Removal. *Chem. Eng. J.* 184, 106–112. doi:10.1016/j.cej.2012.01.009
- Li, W.-J., Li, T.-Y., and Wey, M.-Y. (2021). Preferred Enhancement of Fast-SCR by Mn/CeSiOx Catalyst: Study on Ce/Si Promotion and Shape Dependence. *Chem. Eng. J.* 403, 126317. doi:10.1016/j.cej.2020.126317
- Li, W. B., Yang, X. F., Chen, L. F., and Wang, J. A. (2009). Adsorption/desorption of NOx on MnO₂/ZrO₂ Oxides Prepared in Reverse Microemulsions. *Catal. Today* 148, 75–80. doi:10.1016/j.cattod.2009.03.028
- Li, X., Li, J., Peng, Y., Chang, H., Zhang, T., Zhao, S., et al. (2016). Mechanism of Arsenic Poisoning on SCR Catalyst of CeW/Ti and its Novel Efficient Regeneration Method with Hydrogen. *Appl. Catal. B: Environ.* 184, 246–257. doi:10.1016/j.apcatb.2015.11.042
- Li, Z., Meng, M., Li, Q., Xie, Y., Hu, T., and Zhang, J. (2010). Fe-substituted Nanometric La_{0.9}K_{0.1}Co_{1-x}FexO_{3-δ} Perovskite Catalysts Used for Soot Combustion, NOx Storage and Simultaneous Catalytic Removal of Soot and NOx. *Chem. Eng. J.* 164, 98–105. doi:10.1016/j.cej.2010.08.036
- Lin, H., Li, Y., Shangquan, W., and Huang, Z. (2009). Soot Oxidation and NOx Reduction over BaAl₂O₄ Catalyst. *Combustion and Flame* 156, 2063–2070. doi:10.1016/j.combustflame.2009.08.006
- Lin, X., Li, S., He, H., Wu, Z., Wu, J., Chen, L., et al. (2018). Evolution of Oxygen Vacancies in MnOx-CeO₂ Mixed Oxides for Soot Oxidation. *Appl. Catal. B: Environ.* 223, 91–102. doi:10.1016/j.apcatb.2017.06.071
- Liu, G., and Gao, P.-X. (2011). A Review of NOx Storage/reduction Catalysts: Mechanism, Materials and Degradation Studies. *Catal. Sci. Technol.* 1, 552. doi:10.1039/c1cy00007a
- Liu, J., Zhao, Z., and Duan, C.-m. A.-j. (2008). Simultaneous Removal of NOx and Diesel Soot over Nanometer Ln-Na-Cu-O Perovskite-like Complex Oxide Catalysts. *Appl. Catal. B: Environ.* 78, 61–72. doi:10.1016/j.apcatb.2007.09.001
- Liu, X., Jiang, P., Chen, Y., Wang, Y., Ding, Q., Sui, Z., et al. (2021). A Basic Comprehensive Study on Synergetic Effects Among the Metal Oxides in CeO₂-WO₃/TiO₂ NH₃-SCR Catalyst. *Chem. Eng. J.* 421, 127833. doi:10.1016/j.cej.2020.127833
- Ma, Z., Weng, D., Wu, X., and Si, Z. (2012). Effects of WOx Modification on the Activity, Adsorption and Redox Properties of CeO₂ Catalyst for NOx Reduction with Ammonia. *J. Environ. Sci.* 24, 1305–1316. doi:10.1016/s1001-0742(11)60925-x
- Ndifor, E. N., Garcia, T., Solsona, B., and Taylor, S. H. (2007). Influence of Preparation Conditions of Nano-Crystalline Ceria Catalysts on the Total Oxidation of Naphthalene, a Model Polycyclic Aromatic Hydrocarbon. *Appl. Catal. B: Environ.* 76, 248–256. doi:10.1016/j.apcatb.2007.05.027
- Peng, C., Yu, D., Wang, L., Yu, X., and Zhao, Z. (2021). Recent Advances in the Preparation and Catalytic Performance of Mn-Based Oxide Catalysts with Special Morphologies for the Removal of Air Pollutants. *J. Mater. Chem. A* 9, 12947–12980. doi:10.1039/d1ta00911g
- Qin, D., and Cadet, G. (1997). Quantitative Analysis of Process Streams by On-Line FT-IR Spectrometry. *Anal. Chem.* 69, 1942–1945. doi:10.1021/ac9610826
- Saputra, E., Muhammad, S., Sun, H., Ang, H.-M., Tadó, M. O., and Wang, S. (2014). Shape-controlled Activation of Peroxymonosulfate by Single crystal α-Mn₂O₃ for Catalytic Phenol Degradation in Aqueous Solution. *Appl. Catal. B: Environ.* 154–155, 246–251. doi:10.1016/j.apcatb.2014.02.026
- Serhan, N., Tsolakis, A., Wahbi, A., Martos, F. J., and Golunski, S. (2019). Modifying Catalytically the Soot Morphology and Nanostructure in Diesel

- Exhaust: Influence of Silver De-NO_x Catalyst (Ag/Al₂O₃). *Appl. Catal. B: Environ.* 241, 471–482. doi:10.1016/j.apcatb.2018.09.068
- Shen, Q., Lu, G., Du, C., Guo, Y., Wang, Y., Guo, Y., et al. (2013). Role and Reduction of NO_x in the Catalytic Combustion of Soot over Iron-Ceria Mixed Oxide Catalyst. *Chem. Eng. J.* 218, 164–172. doi:10.1016/j.cej.2012.12.010
- Sinelli, N., Limbo, S., Torri, L., Di Egidio, V., and Casiraghi, E. (2010). Evaluation of Freshness Decay of Minced Beef Stored in High-Oxygen Modified Atmosphere Packaged at Different Temperatures Using NIR and MIR Spectroscopy. *Meat Sci.* 86, 748–752. doi:10.1016/j.meatsci.2010.06.016
- Stec, A. A., Fardell, P., Blomqvist, P., Bustamante-Valencia, L., Saragoza, L., and Guillaume, E. (2011). Quantification of Fire Gases by FTIR: Experimental Characterisation of Calibration Systems. *Fire Saf. J.* 46, 225–233. doi:10.1016/j.firesaf.2011.02.004
- Tan, J., Wei, Y., Sun, Y., Liu, J., Zhao, Z., Song, W., et al. (2018). Simultaneous Removal of NO and Soot Particulates from Diesel Engine Exhaust by 3DOM Fe-Mn Oxide Catalysts. *J. Ind. Eng. Chem.* 63, 84–94. doi:10.1016/j.jiec.2018.02.002
- Urán, L., Gallego, J., Li, W.-Y., and Santamaría, A. (2019). Effect of Catalyst Preparation for the Simultaneous Removal of Soot and NO_x. *Appl. Catal. A: Gen.* 569, 157–169. doi:10.1016/j.apcata.2018.10.029
- Valencia, L. B., Rogaume, T., Guillaume, E., Rein, G., and Torero, J. L. (2009). Analysis of Principal Gas Products during Combustion of Polyether Polyurethane Foam at Different Irradiance Levels. *Fire Saf. J.* 44, 933–940. doi:10.1016/j.firesaf.2009.05.003
- Wang, B., Wang, M., Han, L., Hou, Y., Bao, W., Zhang, C., et al. (2020). Improved Activity and SO₂ Resistance by Sm-Modulated Redox of MnCeSmTiO_x Mesoporous Amorphous Oxides for Low-Temperature NH₃-SCR of NO. *ACS Catal.* 10, 9034–9045. doi:10.1021/acscatal.0c02567
- Wang, K., Qian, L., Zhang, L., Liu, H., and Yan, Z. (2010). Simultaneous Removal of NO_x and Soot Particulates over La_{0.7}Ag_{0.3}MnO₃ Perovskite Oxide Catalysts. *Catal. Today* 158, 423–426. doi:10.1016/j.cattod.2010.06.001
- Wei, Y., Liu, J., Zhao, Z., Duan, A., Jiang, G., Xu, C., et al. (2011). Three-dimensionally Ordered Macroporous Ce_{0.8}Zr_{0.2}O₂-Supported Gold Nanoparticles: Synthesis with Controllable Size and Super-catalytic Performance for Soot Oxidation. *Energy Environ. Sci.* 4, 2959. doi:10.1039/c0ee00813c
- Wu, X., Si, Z., Li, G., Weng, D., and Ma, Z. (2011). Effects of Cerium and Vanadium on the Activity and Selectivity of MnO_x-TiO₂ Catalyst for Low-Temperature NH₃-SCR. *J. Rare Earths* 29, 64–68. doi:10.1016/s1002-0721(10)60403-6
- Xie, S., Dai, H., Deng, J., Liu, Y., Yang, H., Jiang, Y., et al. (2013). Au/3DOM Co₃O₄: Highly Active Nanocatalysts for the Oxidation of Carbon Monoxide and Toluene. *Nanoscale* 5, 11207. doi:10.1039/c3nr04126c
- Xiong, Z.-b., Liu, J., Zhou, F., Liu, D.-y., Lu, W., Jin, J., et al. (2017). Selective Catalytic Reduction of NO with NH₃ over Iron-Cerium-Tungsten Mixed Oxide Catalyst Prepared by Different methods Selective Catalytic Reduction of NO with NH₃ over Iron-Cerium-Tungsten Mixed Oxide Catalyst Prepared by Different Methods. *Appl. Surf. Sci.* 406, 218–225. doi:10.1016/j.apsusc.2017.02.157
- Xu, H., Feng, X., Liu, S., Wang, Y., Sun, M., Wang, J., et al. (2017). Promotional Effects of Titanium Additive on the Surface Properties, Active Sites and Catalytic Activity of W/CeZrO_x Monolithic Catalyst for the Selective Catalytic Reduction of NO_x with NH₃. *Appl. Surf. Sci.* 419, 697–707. doi:10.1016/j.apsusc.2017.05.055
- Xu, H., Li, Y., Xu, B., Cao, Y., Feng, X., Sun, M., et al. (2016). Effectively Promote Catalytic Performance by Adjusting W/Fe Molar Ratio of FeW_x/Ce_{0.68}Zr_{0.32}O₂ Monolithic Catalyst for NH₃-SCR. *J. Ind. Eng. Chem.* 36, 334–345. doi:10.1016/j.jiec.2016.02.024
- Xu, J., Liu, J., Zhao, Z., Xu, C., Zheng, J., Duan, A., et al. (2011). Easy Synthesis of Three-Dimensionally Ordered Macroporous La_{1-x}K_xCoO₃ Catalysts and Their High Activities for the Catalytic Combustion of Soot. *J. Catal.* 282, 1–12. doi:10.1016/j.jcat.2011.03.024
- Yao, X., Chen, L., Cao, J., Chen, Y., Tian, M., Yang, F., et al. (2019). Enhancing the deNO Performance of MnO/CeO₂-ZrO₂ Nanorod Catalyst for Low-Temperature NH₃-SCR by TiO₂ Modification. *Chem. Eng. J.* 369, 46–56. doi:10.1016/j.cej.2019.03.052
- Yoshida, K., Makino, S., Sumlya, S., and Muramat, C. (1989). Simultaneous Reduction of NO_x and Particulate Emissions from Diesel Engine Exhaust. *SAE Tech. Paper* 1, 1994, 2005).
- Yu, D., Ren, Y., Yu, X., Fan, X., Wang, L., Wang, R., et al. (2021a). Facile Synthesis of Birnessite-type K₂Mn₄O₈ and Cryptomelane-type K₂-xMn₈O₁₆ Catalysts and Their Excellent Catalytic Performance for Soot Combustion with High Resistance to H₂O and SO₂. *Appl. Catal. B: Environ.* 285, 119779. doi:10.1016/j.apcatb.2020.119779
- Yu, X., Li, J., Wei, Y., Zhao, Z., Liu, J., Jin, B., et al. (2014). Three-Dimensionally Ordered Macroporous Mn_xCe_{1-x}O₈ and Pt/Mn_{0.5}Ce_{0.5}O₈ Catalysts: Synthesis and Catalytic Performance for Soot Oxidation. *Ind. Eng. Chem. Res.* 53, 9653–9664. doi:10.1021/ie500666m
- Yu, X., Ren, Y., Yu, D., Chen, M., Wang, L., Wang, R., et al. (2021b). Hierarchical Porous K-OMS-2/3dom-M Ti_{0.7}Si_{0.3}O₂ Catalysts for Soot Combustion: Easy Preparation, High Catalytic Activity, and Good Resistance to H₂O and SO₂. *ACS Catal.* 11, 5554–5571. doi:10.1021/acscatal.1c00748
- Yu, X., Wang, L., Chen, M., Fan, X., Zhao, Z., Cheng, K., et al. (2019). Enhanced Activity and Sulfur Resistance for Soot Combustion on Three-Dimensionally Ordered Macroporous-Mesoporous Mn_xCe_{1-x}O₈/SiO₂ Catalysts. *Appl. Catal. B: Environ.* 254, 246–259. doi:10.1016/j.apcatb.2019.04.097
- Yu, X., Zhao, Z., Wei, Y., and Liu, J. (2017). Ordered Micro/macro Porous K-OMS-2/SiO₂ Nanocatalysts: Facile Synthesis, Low Cost and High Catalytic Activity for Diesel Soot Combustion. *Sci. Rep.* 7. doi:10.1038/srep43894
- Zhang, H., Han, J., Niu, X., Han, X., Wei, G., and Han, W. (2011). Study of Synthesis and Catalytic Property of WO₃/TiO₂ Catalysts for NO Reduction at High temperatures Study of Synthesis and Catalytic Property of WO₃/TiO₂ Catalysts for NO Reduction at High Temperatures. *J. Mol. Catal. A: Chem.* 350, 35–39. doi:10.1016/j.molcata.2011.09.001
- Zhang, S., Zhong, Q., Shen, Y., Zhu, L., and Ding, J. (2015a). New Insight into the Promoting Role of Process on the CeO₂-WO₃/TiO₂ Catalyst for NO Reduction with NH₃ at Low-Temperature. *J. Colloid Interf. Sci.* 448, 417–426. doi:10.1016/j.jcis.2015.02.038
- Zhang, Y., Guo, W., Wang, L., Song, M., Yang, L., Shen, K., et al. (2015b). Characterization and Activity of V₂O₅-CeO₂/TiO₂-ZrO₂ Catalysts for NH₃-selective Catalytic Reduction of NO_x. *Chin. J. Catal.* 36, 1701–1710. doi:10.1016/s1872-2067(14)60916-0
- Zhang, Y., Zhu, X., Shen, K., Xu, H., Sun, K., and Zhou, C. (2012). Influence of Ceria Modification on the Properties of TiO₂-ZrO₂ Supported V₂O₅ Catalysts for Selective Catalytic Reduction of NO by NH₃. *J. Colloid Interf. Sci.* 376, 233–238. doi:10.1016/j.jcis.2012.03.001
- Zhu, R., Guo, M., and Ouyang, F. (2008). Simultaneous Removal of Soot and NO_x over Ir-Based Catalysts in the Presence of Oxygen. *Catal. Today* 139, 146–151. doi:10.1016/j.cattod.2008.08.017

Conflict of Interest: The authors declare that the research was conducted in the absence of any commercial or financial relationships that could be construed as a potential conflict of interest.

Publisher's Note: All claims expressed in this article are solely those of the authors and do not necessarily represent those of their affiliated organizations, or those of the publisher, the editors, and the reviewers. Any product that may be evaluated in this article, or claim that may be made by its manufacturer, is not guaranteed or endorsed by the publisher.

Copyright © 2022 Wang, Zhong, Li, Yu, Zhao, Sojka, Kotarba, Wei and Liu. This is an open-access article distributed under the terms of the Creative Commons Attribution License (CC BY). The use, distribution or reproduction in other forums is permitted, provided the original author(s) and the copyright owner(s) are credited and that the original publication in this journal is cited, in accordance with accepted academic practice. No use, distribution or reproduction is permitted which does not comply with these terms.